

Statistics of Dark Matter Substructure: I. Model and Universal Fitting Functions

Fangzhou Jiang[★] & Frank C. van den Bosch

Department of Astronomy, Yale University, New Haven, CT 06511, USA

ABSTRACT

We present a new, semi-analytical model describing the evolution of dark matter subhaloes. The model uses merger trees constructed using the method of Parkinson et al. (2008) to describe the masses and redshifts of subhaloes at accretion, which are subsequently evolved using a simple model for the orbit-averaged mass loss rates. The model is extremely fast, treats subhaloes of all orders, accounts for scatter in orbital properties and halo concentrations, and uses a simple recipe to convert subhalo mass to maximum circular velocity. The model accurately reproduces the average subhalo mass and velocity functions in numerical simulations. The inferred subhalo mass loss rates imply that an average dark matter subhalo loses in excess of 80 percent of its infall mass during its first radial orbit within the host halo. We demonstrate that the total mass fraction in subhaloes is tightly correlated with the ‘dynamical age’ of the host halo, defined as the number of halo dynamical times that have elapsed since its formation. Using this relation, we present universal fitting functions for the evolved and unevolved subhalo mass and velocity functions that are valid for any host halo mass, at any redshift, and for any Λ CDM cosmology.

Key words: methods: analytical — methods: statistical — galaxies: haloes — dark matter

1 INTRODUCTION

Numerical N -body simulations have shown that when two dark matter haloes merge, the less massive progenitor halo initially survives as a self-bound entity, called a subhalo, orbiting within the potential well of the more massive progenitor halo. These subhaloes are subjected to tidal forces and impulsive encounters with other subhaloes causing tidal heating and mass stripping, and to dynamical friction that causes them to lose orbital energy and angular momentum to the dark matter particles of the ‘host’ halo. Depending on its orbit, density profile, and mass, a subhalo therefore either survives to the present day or is disrupted; the operational distinction being whether a self-bound entity remains or not.

Characterizing the statistics and properties of dark matter subhaloes is of paramount importance for various areas of astrophysics. First of all, subhaloes are believed to host satellite galaxies, and the abundance of satellite galaxies is therefore directly related to that of subhaloes. This basic idea underlies the popular technique of subhalo abundance matching (e.g., Vale & Ostriker 2004; Conroy et al. 2006, 2007; Guo et al. 2011; Hearin et al. 2013) and

has given rise to two problems in our understanding of galaxy formation: the “missing satellite” problem (Moore et al. 1999; Klypin et al. 1999) and the “too big to fail” problem (Boylan-Kolchin et al. 2011). Secondly, substructure is also important in the field of gravitational lensing, where it can cause time-delays (e.g., Keeton & Moustakas 2009) and flux-ratio anomalies (Metcalf & Madau 2001; Bradač et al. 2002; Dalal & Kochanek 2002), and for the detectability of dark matter annihilation, where the clumpiness due to substructure is responsible for a ‘boost factor’ (e.g., Diehm et al. 2007; Pieri et al. 2008; Giocoli et al. 2008b). Finally, the abundance and properties of dark matter substructure controls the survivability of fragile structures in dark matter haloes, such as tidal streams and/or galactic disks (Tóth & Ostriker 1992; Taylor & Babul 2001; Ibata et al. 2002; Carlberg 2009).

The most common statistic used to describe the substructure of dark matter haloes is the subhalo mass function (hereafter SHMF), $dN/d\ln(m/M)$, which expresses the (average) number of subhaloes of mass m per host halo of mass M , per logarithmic bin of m/M . Following van den Bosch, Tormen & Giocoli (2005), we will distinguish two different SHMFs; the *unevolved* SHMF, where m is the mass of the subhalo *at accretion*, and the *evolved* SHMF, where m reflects the mass of the surviving, self-bound entity at the

[★] E-mail:fangzhou.jiang@yale.edu

present day, which is reduced with respect to that at accretion due to mass stripping.

The SHMFs of dark matter haloes have been studied using two complementary techniques; N -body simulations (e.g., Tormen 1997; Tormen, Diaferio & Syer 1998; Moore et al. 1998, 1999; Klypin et al. 1999a,b; Ghigna et al. 1998, 2000; Stoehr et al. 2002; De Lucia et al. 2004; Diemand, Moore & Stadel 2004; Gill et al. 2004a,b; Gao et al. 2004; Reed et al. 2005; Kravtsov et al. 2004; Giocoli et al. 2008a, 2010; Weinberg et al. 2008) and semi-analytical techniques based on the extended Press-Schechter (EPS; Bond et al. 1991) formalism (e.g., Taylor & Babul 2001, 2004, 2005a,b; Benson et al. 2002; Taffoni et al. 2003; Oguri & Lee 2004; Zentner & Bullock 2003; Peñarrubia & Benson 2005; Zentner et al. 2005; van den Bosch et al. 2005; Gan et al. 2010; Yang et al. 2011; Purcell & Zentner 2012). Both methods have their own pros and cons. Numerical simulations have the virtue of including all relevant, gravitational physics related to the assembly of dark matter haloes, and the evolution of the subhalo population. However, they are also extremely CPU intensive, and the results depend on the mass- and force-resolution adopted. In addition, there is some level of arbitrariness in how to identify haloes and subhaloes in the simulations. In particular, different (sub)halo finders applied to the same simulation output typically yield subhalo mass functions that differ at the 10-20 percent level (Knebe et al. 2011, 2013; Onions et al. 2012) or more (van den Bosch & Jiang 2014). Semi-analytical techniques, on the other hand, don't suffer from issues related to subhalo identification or force resolution, and are significantly faster, but their downside is that the relevant physics is only treated approximately.

All semi-analytical methods require two separate ingredients: halo merger trees, which describe the hierarchical assembly of dark matter haloes, and a treatment of the various physical processes that cause the subhalo population to evolve (dynamical friction, tidal heating and stripping, impulsive encounters). To properly account for all these processes, which depend strongly on the orbital properties, requires a detailed integration over all individual subhalo orbits. This is complicated by the fact that the mass of the parent halo evolves with time. If the mass growth rate is sufficiently slow, the evolution may be considered adiabatic, thus allowing the orbits of subhaloes to be integrated analytically despite the non-static nature of the background potential. This principle is exploited in many of the semi-analytical based models listed above. In reality, however, haloes grow hierarchically through (major) mergers, making the actual orbital evolution highly non-linear.

In order to sidestep these difficulties, van den Bosch, Tormen & Giocoli (2005; hereafter B05) considered the *average* mass loss rate of dark matter subhaloes, where the average is taken over the entire distribution of orbital configurations (energies, angular momenta, and orbital phases). This removes the requirement to actually integrate individual orbits, allowing for an extremely fast calculation of the evolved subhalo mass function. B05 adopted a simple functional form for the average mass loss rate, which had two free parameters which they calibrated by comparing the resulting subhalo mass functions to those obtained using numerical simulations. In a subsequent paper, Giocoli, Tormen & van den Bosch (2008; hereafter G08), directly measured

the average mass loss rate of dark matter subhaloes in numerical simulations. They found that the functional form adopted by B05 adequately describes the average mass loss rates in the simulations, but with best-fit values for the free parameters that are substantially different. G08 argued that this discrepancy arises from the fact that B05 used the ‘N-branch method with accretion’ of Somerville & Kolatt (1999; hereafter SK99) to construct their halo merger trees, which results in an unevolved subhalo mass function that is significantly different from what is found in the simulations. This was recently confirmed by the authors in a detailed comparison of merger tree algorithms (Jiang & van den Bosch 2014a; hereafter JB14). Note that this same SK99 method has also been used by most of the other semi-analytical models for dark matter substructure, including Taylor & Babul (2004, 2005a,b), Zentner & Bullock (2003), Zentner et al. (2005) and even the recent study by Purcell & Zentner (2012).

In this series of papers we use an overhauled version of the semi-analytical method pioneered by B05 to study the statistics of dark matter subhaloes in unprecedented detail. In particular, we extent and improve upon B05 by (i) using halo merger trees constructed with the more reliable method of Parkinson, Cole & Helly (2008), (ii) evolving subhaloes using the improved mass-loss model of G08 and accounting for stochasticity in the mass-loss rates due to the scatter in orbital properties and halo concentrations, (iii) considering the entire hierarchy of dark matter subhaloes (including sub-subhaloes, sub-sub-subhaloes, etc.), and (iv) predicting not only the masses of subhaloes but also their maximum circular velocities, V_{\max} . In this paper, the first in the series, we present the improved semi-analytical model, followed by a detailed study of the (average) subhalo abundance as function of mass and maximum circular velocity including a presentation of universal fitting functions. In Paper II (van den Bosch & Jiang 2014) we present a more detailed comparison of the model predictions with simulation results, paying special attention to the large discrepancies among different simulation results that arise from the use of different subhalo finders. Finally, in Paper III (Jiang & van den Bosch; in preparation) we exploit our semi-analytical model to quantify the halo-to-halo variation of populations of dark matter subhaloes.

This paper is organized as follows. We start in §2 with a detailed description of our semi-analytical model, including the construction of halo merger trees (§2.1), an updated model for the average mass loss rate of subhaloes (§2.2), and a description of how we convert (sub)halo masses to their corresponding V_{\max} (§2.3). In §3 we demonstrate that the model can accurately reproduce both the subhalo mass and velocity functions obtained from numerical simulations, after tuning our single free model parameter, and we discuss the scalings with host halo mass and redshift. §4 presents accurate, universal fitting functions for the average subhalo mass and velocity functions that are valid for any host halo mass, redshift and Λ CDM cosmology. In §5 we discuss implications of our inferred subhalo mass loss rates, and we summarize our results in §6.

Throughout we use m and M to refer to the masses of subhaloes and host haloes, respectively, use \ln and \log to indicate the natural logarithm and 10-based logarithm, respectively, and express units that depend on the Hubble constant in terms of $h = H_0/(100 \text{ km s}^{-1} \text{ Mpc}^{-1})$.

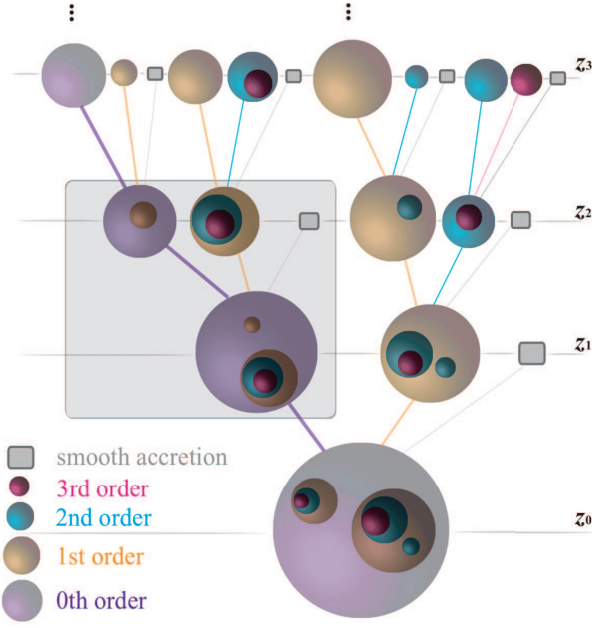


Figure 1. Illustration depicting the anatomy of a merger tree for a host halo (purple sphere at the bottom) at redshift $z = z_0$. The purple spheres to the left illustrate the assembly history of the main progenitor. We refer to these as ‘zeroth-order’ progenitors, and they accrete ‘first-order’ progenitors, which end up as (first-order) subhaloes at $z = z_0$. In turn, these first-order progenitors accrete second-order progenitors which end-up as second-order subhaloes (sub-subhaloes) at $z = z_0$, etc. The size of a sphere is proportional to its mass, while its color reflects its order, as indicated. The large, shaded box highlights a single branching point in the tree structure, which shows a descendant halo plus its single-time-step progenitors. The small shaded boxes present at each branching point reflect ‘smooth accretion’, as defined in the text.

2 MODEL DESCRIPTION

The goal of this series of papers is to present a study of unprecedented detail regarding the statistics of dark matter subhaloes. To that extent we use an improved and extended version of the semi-analytical model of B05 which computes the masses of subhaloes for a particular realization of a host halo’s mass assembly history. In what follows we present a detailed description of the model, including a discussion of how and where we make improvements, and add extensions, with respect to the B05 model.

2.1 Halo Merger Trees

The backbone of the B05 model, and of any other semi-analytical model for the substructure of dark matter haloes, is halo merger trees. These describe the hierarchical mass assembly of dark matter haloes, and therefore yield the masses and redshifts at which dark matter subhaloes are accreted into their hosts.

Before describing the construction of our merger trees, it is useful to introduce some terminology that is used throughout this paper. Fig. 1 shows a schematic representation of a merger tree. We refer to the halo at the base of the tree (i.e., the large purple halo at $z = z_0$) as the *host*

halo. For each individual branching point along the tree (one example is highlighted in Fig. 1), the end-product of the merger event is called the *descendant halo*, while the haloes that merge are called the *progenitors*. The *main progenitor* of a descendant halo is the progenitor that contributes the most mass. For example, for the branching point highlighted in Fig. 1, the purple halo at $z = z_2$ is the main progenitor of its descendant at $z = z_1$. The *main branch* of the merger tree is defined as the branch tracing the main progenitor of the main progenitor of the main progenitor, etc. (i.e., the branch connecting the purple haloes). Note that the main progenitor halo at redshift z is not necessarily the most massive progenitor at that redshift. Throughout we shall occasionally refer to the main progenitor haloes of a given host halo as its zeroth-order progenitors, while the mass history, $M(z)$, along this branch is called the *mass assembly history* (MAH). Haloes that accrete directly onto the main branch are called first-order progenitors, or, after accretion, first-order subhaloes. Similarly, haloes that accrete directly onto first-order progenitors are called second-order progenitors, and they end up at $z = z_0$ as second-order subhaloes (or sub-subhaloes) of the host halo. The same logic is used to define higher-order progenitors and subhaloes, as illustrated in Fig. 1. An n^{th} -order (sub)halo that hosts an $(n+1)^{\text{th}}$ -order subhalo is called a *parent* halo of the $(n+1)^{\text{th}}$ -order subhalo. Throughout, we define (sub)halo masses such that the mass of an n^{th} -order parent halo *includes* the masses of its subhaloes of order $n+1$; we refer to this as the *inclusive* definition of subhalo mass. Most subhalo finders used to analyze N -body simulations use the same inclusive definition of subhalo mass, though not all of them (see Paper II for a detailed discussion).

We construct our merger trees using the EPS formalism, which has the advantage over using numerical simulations that it is not hampered by ambiguities having to do with the identification and linking of (sub)haloes. EPS provides the progenitor mass function (hereafter PMF), $n_{\text{EPS}}(M_p, z_1 | M_0, z_0)$, describing the ensemble-average number, $n_{\text{EPS}}(M_p, z_1 | M_0, z_0) dM_p$, of progenitors of mass M_p that a descendant halo of mass M_0 at redshift z_0 has at redshift $z_1 > z_0$. Starting from some target host halo mass M_0 at z_0 , one can use this PMF to draw a set of progenitor masses $M_{p,1}, M_{p,2}, \dots, M_{p,N}$ at some earlier time $z_1 = z_0 + \Delta z$, where $\sum_{i=1}^N M_{p,i} = M_0$ in order to assure mass conservation. The time-step Δz used sets the ‘temporal resolution’ of the merger tree, and may vary along the tree. This procedure is then repeated for each progenitor with mass $M_{p,i} > M_{\text{res}}$, thus advancing ‘upwards’ along the tree. The minimum mass M_{res} sets the ‘mass resolution’ of the merger tree and is typically expressed as a fraction of the final host mass M_0 . The small shaded boxes in Fig. 1, present at each branching, reflect the mass accreted by the descendant halo in the form of smooth accretion (i.e., not part of any halo) or in the form of progenitor haloes with masses $M_p < M_{\text{res}}$. Throughout we shall refer to this component as *smooth accretion*.

Haloes at the top of the tree that have no progenitors with mass $M_p > M_{\text{res}}$ are called the *leave* haloes of the tree, and the mass evolution of a leave halo down to $z = 0$ is called the halo’s *trajectory*. Only one trajectory per tree corresponds to a host halo (namely that of the main progenitor), while all other trajectories end up as sub-haloes at

$z = 0$ (of different orders). The moment a halo is for the first time accreted into a more massive halo (i.e., transits from being a host halo to a sub-halo) is called the halo's *accretion time*, t_{acc} , and its mass at that time is called the *accretion mass*, for which we use m_{acc} or m_{acc} without distinction. Throughout we use the subscript '0' to refer to properties at redshift $z = z_0$ (typically we adopt $z_0 = 0$); Hence, m_0 is the $z = z_0$ mass of a sub-halo, which differs from m_{acc} due to mass loss (see §2.2 below). In what follows we refer to the mass functions $dN/d \ln(m_0/M_0)$ and $dN/d \ln(m_{\text{acc}}/M_0)$ as the *evolved* and *unevolved* SHMFs of a host halo of mass M_0 , respectively.

B05 constructed EPS merger trees using the SK99 method, but only up to first order; i.e., they only considered first-order subhaloes, and therefore did not require merger trees that resolve the assembly histories of first-order progenitors. We extend this by using full merger trees, thus allowing us to study the statistics of subhaloes of all orders. In addition, we also improve upon B05 by using another method to construct our merger trees. In JB14 we tested and compared a number of different Monte Carlo algorithms for constructing EPS-based merger trees, including SK99. We showed that the SK99-method results in (i) haloes that assemble too late, (ii) merger rates that are too high by factors of two to three (see also Fakhouri & Ma 2008; Genel et al. 2009), and (iii) unevolved subhalo mass functions that are much too high, especially for subhaloes with $m_{\text{acc}} \sim M_0/100$. As first pointed out by G08, and as discussed in more detail in JB14, this explains why B05 inferred an average subhalo mass loss rate that is too high. It also implies that other models for dark matter substructure that are based on the SK99 algorithm (Taylor & Babul 2004, 2005; Zentner & Bullock 2003; Zentner et al. 2005; Purcell & Zentner 2012), are likely to suffer from similar systematic errors.

As we demonstrated in JB14, the merger tree algorithm developed by Cole et al. (2000), which is used in the semi-analytical substructure models of Benson et al. (2002) and Peñarrubia & Benson (2005), has similar shortcomings as SK99, albeit at a significantly reduced level. However, it still overpredicts the unevolved SHMF by ~ 40 percent, and is therefore not well suited to model the population of dark matter subhaloes. Of all the methods tested by JB14, the one that clearly stood out as the most reliable is that of Parkinson et al. (2008; hereafter P08). The P08 algorithm is a modification of the binary algorithm of Cole et al. (2000), in which the PMF is modified with respect to the EPS prediction to match results from the Millennium simulation (see Cole et al. 2008). As shown in JB14, the P08 algorithm yields merger rates and unevolved SHMFs that are in excellent agreement with simulation results within the errors. Hence, in this paper we improve upon B05 by using merger trees constructed with the P08 algorithm. Throughout we always adopt a mass resolution of $\psi_{\text{res}} \equiv M_{\text{res}}/M_0 = 10^{-5}$ unless mentioned otherwise, and construct the merger trees using the time stepping advocated in Appendix A of P08 (which roughly corresponds to $\Delta z \sim 10^{-3}$; somewhat finer/coarser at high/low redshift). In order to speed up the code, and to reduce memory requirements, we down-sample the time resolution of each merger tree by registering progenitor haloes every time step $\Delta t = 0.1 t_{\text{ff}}(z)$. Here $t_{\text{ff}}(z) \propto (1+z)^{-3/2}$ is the free-fall time for a halo with an overdensity of 200 at

redshift z . Since the orbital time of a subhalo is of order the free-fall time, there is little added value in resolving merger trees at higher time resolution than this. We have verified that indeed our results do not change if we use merger trees with a smaller time step.

2.2 Subhalo Mass Evolution

The next ingredient in the semi-analytical method is a model for the mass evolution of the subhalo as it orbits its host halo. This is governed by tidal stripping, tidal heating, dynamical friction, and the impulsive heating due to high-speed encounters with other substructures. Consequently, the mass evolution of a subhalo can vary dramatically along an orbit, and also depends strongly on the orbital energy and angular momentum (see e.g., Taffoni et al. 2003; Taylor & Babul 2004; Penarrubia & Benson 2005; Zentner et al. 2005; Gan et al. 2010).

The unique aspect of the B05 approach is that it considers the *average* mass loss rate of a dark matter subhalo, where the average is taken over all orbital energies, eccentricities and phases. Using the fact that dark matter haloes have a universal density profile (e.g., Navarro, Frenk & White 1997), and that the distribution of orbital properties of infalling subhaloes have only a mild dependence on parent halo mass (e.g. Zentner et al. 2005; Wang et al. 2005; Khochfar & Burkert 2006; Wetzel 2011), this average mass loss rate, to first order, only depends on the instantaneous masses of the subhalo, m , and parent halo, M . In fact, B05 postulated that the dependence on parent halo mass only enters through the (instantaneous) mass ratio m/M , i.e.,

$$\dot{m} = -\mathcal{A} \frac{m}{\tau_{\text{dyn}}} \left(\frac{m}{M} \right)^{\zeta}. \quad (1)$$

Here the negative sign is to emphasize that m is expected to decrease with time, \mathcal{A} and ζ are two free parameters describing the normalization and mass dependence of the subhalo mass loss rate, respectively, and

$$\begin{aligned} \tau_{\text{dyn}}(z) &= \sqrt{\frac{3\pi}{16G\bar{\rho}_{\text{h}}(z)}} \\ &= 1.628 h^{-1} \text{Gyr} \left[\frac{\Delta_{\text{vir}}(z)}{178} \right]^{-1/2} \left[\frac{H(z)}{H_0} \right]^{-1} \end{aligned} \quad (2)$$

is the halo's dynamical time, with $H(z)$ the Hubble parameter, and $\Delta_{\text{vir}}(z)$ the virial parameter that expresses the average density of a virialized dark matter halo, $\bar{\rho}_{\text{h}}$, at redshift z in units of the critical density at that redshift. Throughout this paper we adopt the fitting function for $\Delta_{\text{vir}}(z)$ given by Bryan & Norman (1998).

For a subhalo embedded in a static parent halo ($\dot{M} = 0$) this yields

$$m(t+\Delta t) = \begin{cases} m(t) \exp(-\Delta t/\tau) & \text{if } \zeta = 0 \\ m(t) \left[1 + \zeta \left(\frac{m}{M} \right)^{\zeta} \left(\frac{\Delta t}{\tau} \right) \right]^{-1/\zeta} & \text{otherwise} \end{cases} \quad (3)$$

where $\tau = \tau(z) \equiv \tau_{\text{dyn}}(z)/\mathcal{A}$ is the characteristic mass-loss time scale at redshift z .

Although the subhalo mass loss rate in a static halo is a well defined concept, in reality the parent mass M increases with time due to the accretion of matter and other

subhaloes. Following B05, we utilize the discrete time stepping of the merger tree to evolve both m and M . At the beginning of each time step the parent halo is assumed to instantaneously increase its mass as described by the merger tree ($\dot{M} > 0, \dot{m} = 0$), while in between two time steps we set $\dot{M} = 0$ and evolve the subhalo mass, m , according to Eq. (3). In what follows we consider it understood that m and M depend on time, without having to write this time-dependence explicitly.

B05 adopted the subhalo mass loss model given by Eqs. (1) and (2) and tuned the free parameters, \mathcal{A} and ζ , such that their evolved SHMF matched that obtained from simulations. This resulted in $\mathcal{A} = 23.7$, corresponding to a characteristic mass-loss time scale at $z = 0$ equal to $\tau_0 = 0.13\text{Gyr}$, and $\zeta = 0.36$. Using high-resolution N -body simulations, G08 computed the *average* mass loss rates of dark matter subhaloes as a function of both halo mass and redshift. They found that the functional forms of Eqs. (1) and (2) adequately describes the simulation results, but with best-fit values $\mathcal{A} = 1.54^{+0.52}_{-0.31}$ (corresponding to $\tau_0 = (2.0 \pm 0.5)\text{Gyr}$) and $\zeta = 0.07 \pm 0.03$ that are very different from those obtained in B05. In particular, the much smaller value for \mathcal{A} implies significantly lower mass loss rates. As discussed in G08, this is a manifestation of the shortcomings of the SK99 algorithm used by B05 to construct their merger trees; in order to match the evolved SHMF in the simulations, B05 had to adopt higher mass loss rates to compensate for the overabundance of accreted subhaloes.

In this paper we adopt $\zeta = 0.07$ and treat \mathcal{A} as a free parameter, which we tune by fitting our evolved subhalo mass functions to simulation results. As we show, mainly because we now use more accurate halo merger trees, the resulting value of \mathcal{A} (1.34) is in excellent agreement with the simulation results of G08.

2.2.1 Subhalo Mass Loss Rates; a toy model

An important goal of this work (discussed in detail in Paper II) is to assess the halo-to-halo variance of subhalo statistics. The main source of this variance is the scatter in mass accretion histories (i.e., halo-to-halo variance in the accretion masses and accretion redshifts of subhaloes), which is accounted for via our merger trees. However, another important source of scatter is that due to variance in the orbital properties; orbits with more negative orbital energy, or with smaller angular momentum, will have a smaller pericenter and therefore experience more tidal stripping. In addition, since the tidal radius of a subhalo depends on the density profiles of host halo and subhalo, a third source of scatter is the variance in halo concentrations, of both the host halo and the subhalo. Using numerical simulations, G08 indeed found a substantial scatter in the subhalo mass loss rates, which is well represented by a log-normal with a standard deviation of $\sigma_{\log(\dot{m}/M)} \sim 0.25$. However, G08 measured the mass loss rates averaged over a time step of $\sim 0.1\text{Gyr}$, which is much shorter than an orbital period. Hence, their mass loss rates are not truly orbit-averaged, and their scatter contains a contribution due to variations in \dot{m}/M along individual orbits. In order to gauge the scatter in *orbit-averaged* subhalo mass loss rates due to the variance in orbital prop-

erties and halo concentrations we consider a simple, but insightful, toy model.

Consider a subhalo of mass m on an orbit of energy E and angular momentum L (both per unit mass) inside a host halo of mass M . In what follows we use r and R to refer to halo-centric radii in the subhalo and host halo, respectively. As the subhalo orbits within the potential of the host halo, it experiences dynamical friction, tidal heating and tidal stripping, all of which contribute to the subhalo losing mass. Most of this mass loss occurs close to the orbit's pericenter, R_p , where the tidal field of the host is strongest. Hence, we may approximate the orbit averaged mass loss rate of a subhalo as

$$\dot{m} = \frac{m - m(r_t)}{T_r}, \quad (4)$$

where r_t is the subhalo's tidal radius at the orbit's pericenter, T_r is the radial orbital period, and $m(r)$ is the subhalo mass enclosed within radius r . Hence, we assume that all the mass beyond the tidal radius of the subhalo at the orbit's pericenter is stripped from the subhalo in one radial period. This is admittedly a crude, and poorly justified, assumption, but as we will show below, it yields results in close agreement with numerical simulations.

Throughout we assume that both host haloes and subhaloes are defined as spheres with an average density, inside their virial radii, given by $\bar{\rho}_h = \Delta_{\text{crit}}(z)\rho_{\text{crit}}(z)$, and with an NFW density profile (Navarro, Frenk & White 1997). Hence, their enclosed mass profile is

$$M(R) = M \frac{f(cR/R_{\text{vir}})}{f(c)}, \quad (5)$$

with c the halo concentration parameter, R_{vir} the halo virial radius, and $f(x) = \ln(1+x) - x/(1+x)$. We assume that, at fixed halo mass, the concentrations follow a log-normal distribution with standard deviation $\sigma_{\log c} \simeq 0.12$ (e.g., Macciò et al. 2010) and with a *median* that depends on halo mass and redshift according to

$$c(M, z) = \frac{4.67}{1+z} \left(\frac{M(z)}{10^{14} h^{-1} \text{M}_{\odot}} \right)^{-0.11} \quad (6)$$

(Neto et al. 2007).

With the mass profile of the host halo specified, we can determine the apocenter, R_a and pericenter, R_p of the subhalo's orbit, by solving for the roots of

$$\frac{1}{R^2} + \frac{2[\Phi(R) - E]}{L^2} = 0 \quad (7)$$

(Binney & Tremaine 2008). Here

$$\Phi(R) = -V_{\text{vir}}^2 \frac{\ln(1 + cR/R_{\text{vir}})}{f(c)R/R_{\text{vir}}} \quad (8)$$

is the gravitational potential of the NFW host halo, with $V_{\text{vir}} = \sqrt{GM/R_{\text{vir}}}$ the host halo's virial velocity. The radial orbital period is given by

$$T_r = 2 \int_{R_p}^{R_a} \frac{dR}{\sqrt{2[E - \Phi(R)] - L^2/R^2}}, \quad (9)$$

(Binney & Tremaine 2008), and the tidal radius of the subhalo at $R = R_p$ is obtained by solving

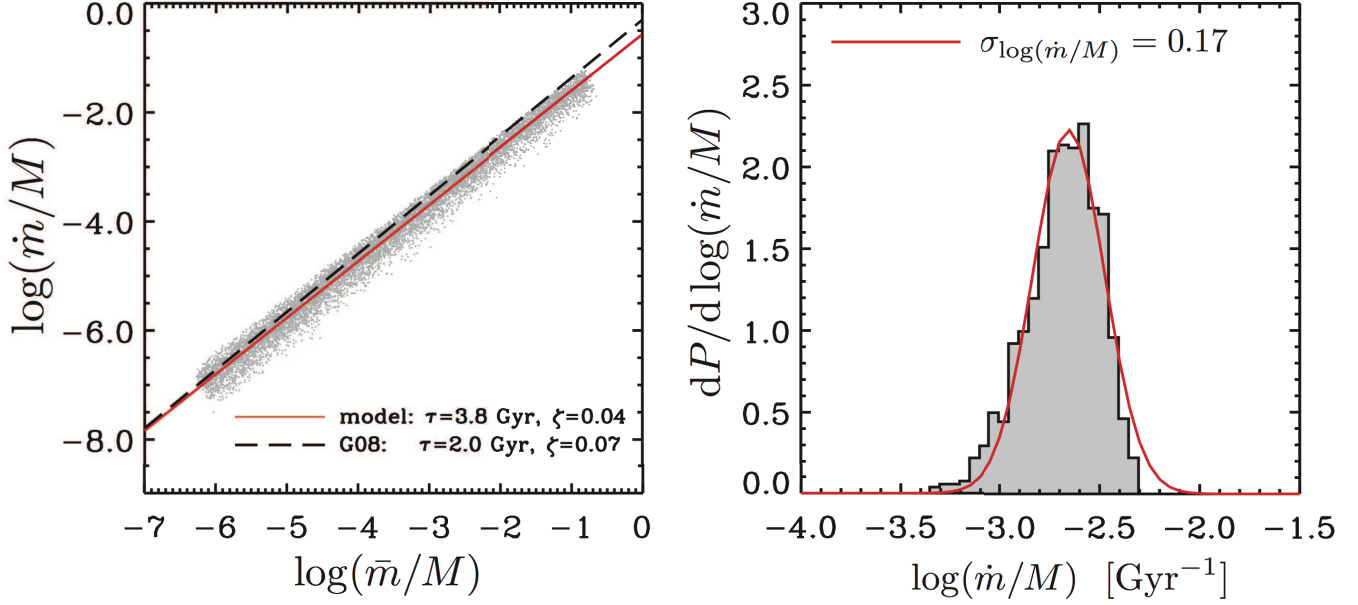


Figure 2. Results obtained from the toy model. *Left Panel:* orbit-averaged mass-loss rates, \dot{m} , as a function of the orbit-averaged subhalo mass, \bar{m} , for a host halo of mass $M = 10^{13} h^{-1} M_{\odot}$ at $z = 0$. Grey dots represent the 10,000 individual Monte-Carlo realizations. The solid red line is the best-fit to the median, which corresponds to Eq. (1)-(2) with $\mathcal{A} = 0.81$ and $\zeta = 0.04$. The dashed black line represents the average subhalo mass-loss rates of G08, as measured from numerical simulations, which has $\mathcal{A} = 1.54$ and $\zeta = 0.07$. *Right Panel:* the distribution of orbit-averaged mass-loss rates at $\log(\bar{m}/M) = -2$. The distribution can be approximated as a log-normal distribution with dispersion $\sigma_{\log(\dot{m}/M)} = 0.17$ (red curve).

$$r_t = R_p \left[\frac{m(r_t)/M(R_p)}{2 + \frac{\Omega_p^2 R_p^3}{G M(R_p)} - \frac{d \ln M}{d \ln R} \Big|_{R_p}} \right]^{1/3}, \quad (10)$$

(e.g., von Hoerner 1957; King 1962; Taylor & Babul 2001), where

$$\Omega_p = L/R_p^2 \quad (11)$$

is the instantaneous angular speed at pericenter.

The final ingredient for our toy model is the probability distribution, $\mathcal{P}(E, L)$, for the orbital energies and angular momenta of dark matter subhaloes. For convenience, we characterize E and L via the radius of a circular orbit, R_c , and the orbital circularity, η . The relations between (E, L) and (R_c, η) are given by

$$E = \frac{1}{2} V_c^2 + \Phi(R_c), \quad (12)$$

with V_c the circular speed at $R = R_c$, and

$$L = \eta L_c(E) \quad (13)$$

with $L_c(E) = R_c V_c$ the maximum angular momentum for an orbit of energy E . Using high-resolution numerical simulations, Zentner et al. (2005) has shown that the circularity distribution for the orbits of subhaloes at infall is well fit by

$$P(\eta) \propto \eta^{1.22} (1 - \eta)^{1.22}. \quad (14)$$

Zentner et al. (2005) also showed that the distribution of R_c for the infalling subhaloes is well approximated by a uniform distribution covering the range $[0.6 R_{\text{vir}}, R_{\text{vir}}]$, i.e.,

$$\mathcal{P}(R_c) = \begin{cases} 5/3 & \text{if } 0.6 \leq R_c/R_{\text{vir}} \leq 1.0 \\ 0 & \text{otherwise} \end{cases} \quad (15)$$

For our toy model we follow Gan et al. (2010) and assume that the probability distribution for R_c and η is separable, i.e., $\mathcal{P}(R_c, \eta) = \mathcal{P}(R_c) \mathcal{P}(\eta)$, and draw the values for R_c and η from Eqs. (15) and (14), respectively[†].

Using this toy model, we compute orbit-averaged mass loss rates for large ensembles of subhaloes as follows. For a given host halo mass, we first draw a subhalo mass, m , from a uniform distribution on the interval $\log(m/M) \in [-6.0, -0.5]$.[‡] Next we draw concentrations for both the host halo and subhalo, using the log-normal distribution described above, as well as values for the orbital energy and angular momentum of the subhalo. These are used to compute the radial orbital period, T_r , and the subhalo's tidal radius, r_t , from which we ultimately compute the mass loss rate using Eq. (4). The left-hand panel of Fig. 2 shows the resulting orbit-averaged mass loss rates, \dot{m}/M , as function of the orbit averaged subhalo mass, \bar{m}/M , where $\bar{m} = m - (\dot{m} T_r)/2$. Both have been normalized by the host halo mass, M , for convenience. The dots are the results obtained for our toy model, using 10,000 subhaloes for a host halo of mass $M = 10^{13} h^{-1} M_{\odot}$. We find that our model results are well fit by Eqs. (1)-(2) with $\mathcal{A} = 0.81$ and $\zeta = 0.04$, which is shown as the solid line. Hence, our toy model lends further support to the functional form of the average subhalo mass loss rate introduced by B05. For comparison, the dashed line

[†] Actually, we sample the circularities from the modified distribution, $\mathcal{P}(\eta) d\eta = \frac{\pi}{2} \sin(\pi\eta) d\eta$, which accurately fits Eq. (14) and has the advantage that it allows values of η to be drawn by direct inversion.

[‡] We have verified that drawing subhalo mass from the unevolved SHMF instead does not alter any of the results.

is the best-fit relation obtained by G08 from their numerical simulations. As is apparent, the latter is somewhat steeper ($\zeta = 0.07$), and implies somewhat larger mass loss rates ($\mathcal{A} = 1.54$). We believe that this discrepancy between our toy model and the G08 simulation results is most likely due to the fact that our toy model ignores dynamical friction, which reduces the orbit's pericentric distance as well as the radial orbital period, both of which will boost the mass loss rate. Since dynamical friction is more important for more massive subhaloes, taking dynamical friction into account is likely to increase both ζ and \mathcal{A} , bringing the toy model in better agreement with the simulation results.

As mentioned above, the main goal of the toy model is to gain some insight regarding the scatter in \dot{m}/M that arises due to variance in the orbital properties and halo concentrations. The right panel of Fig. 2 plots the distribution of normalized subhalo mass loss rates, $d\mathcal{P}/d(\dot{m}/M)$, at fixed $\dot{m}/M = 0.01$, which is well fit by a log-normal with a standard deviation $\sigma_{\log(\dot{m}/M)} = 0.17$ (red curve). Note that this scatter is substantially smaller than the $\sigma_{\log(\dot{m}/M)} \simeq 0.25$ measured by G08 from their simulations, as expected. In fact, our results imply that the contribution to the variance measure by G08 due to variations in \dot{m}/M along an orbit are of the order of $\sqrt{0.25^2 - 0.17^2} \simeq 0.18$, comparable to the scatter that arises from variations in orbital properties, which is roughly what one expects. Since our model requires orbit-averaged mass loss rates, we will model the scatter in \dot{m}/M using a log-normal distribution with $\sigma_{\log(\dot{m}/M)} = 0.17$ (see §2.4 below).

2.3 Converting Mass to Maximum Circular Velocity

In addition to subhalo mass, we also want the semi-analytical model to be able to yield the maximum circular velocity V_{\max} for each of its subhaloes. The maximum circular velocity of a halo of mass M depends on its density distribution. In the case of NFW haloes

$$V_{\max} = 0.465 V_{\text{vir}} \sqrt{\frac{c}{\ln(1+c) - c/(1+c)}}, \quad (16)$$

where

$$V_{\text{vir}} = 159.43 \text{ km s}^{-1} \left(\frac{M}{10^{12} h^{-1} \text{ M}_{\odot}} \right)^{1/3} \left[\frac{H(z)}{H_0} \right]^{1/3} \left[\frac{\Delta_{\text{vir}}(z)}{178} \right]^{1/6}, \quad (17)$$

is the virial velocity of a dark matter halo of virial mass M at redshift z . It is well known that the concentration of a dark matter halo is strongly correlated with its MAH, in the sense that haloes that assemble earlier are more concentrated (e.g., Navarro et al. 1997; Wechsler et al. 2002; Ludlow et al. 2013). We use the model of Zhao et al. (2009), according to which

$$c(M, t) = 4.0 \left[1 + \left(\frac{t}{3.75 t_{0.04}} \right)^{8.4} \right]^{1/8}. \quad (18)$$

Here $t_{0.04}$ is the proper time at which the host halo's main progenitor gained 4 percent of its mass at proper time t , which we extract from the halo's merger tree, as described below.

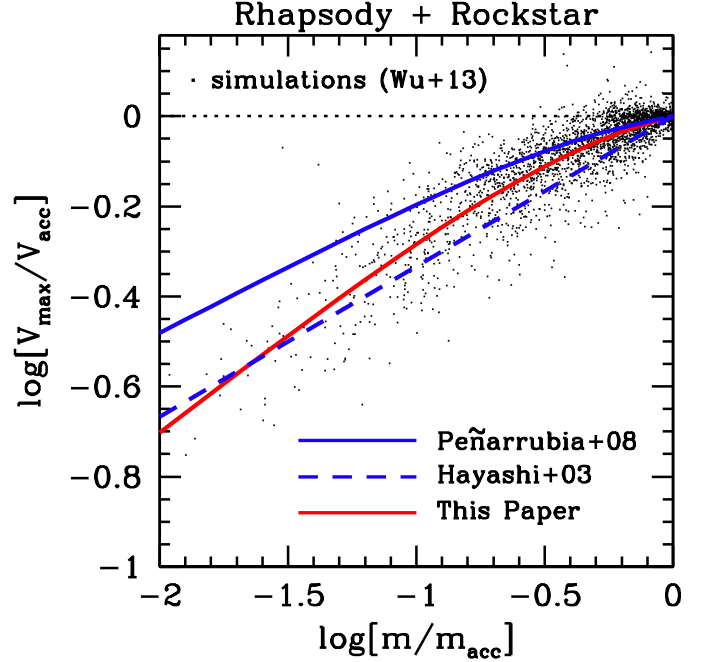


Figure 3. The ratio V_{\max}/V_{acc} as function of m/m_{acc} for 2735 subhaloes in the Rhapsody simulations (black dots). The solid, red line is the best-fit equation of the form (19) with best-fit parameter $(\eta, \mu) = (0.44, 0.60)$. This is the relation we use throughout to compute the maximum circular velocities of dark matter subhaloes in our semi-analytical model. The solid and dashed blue curves are the best-fit results of Hayashi et al. (2003) and Peñarrubia et al. (2010), and are shown for comparison.

For subhaloes, we use the results of Hayashi et al. (2003) and Peñarrubia et al. (2008, 2010), who, using idealized numerical simulations, have shown that the evolution of the maximum circular velocity of a dark matter subhalo depends solely on the total amount of mass stripped, and not on the details of how or when that mass is stripped. Following Peñarrubia et al. (2008) we therefore write

$$V_{\max} = 2^{\mu} V_{\text{acc}} \frac{(m/m_{\text{acc}})^{\nu}}{(1 + m/m_{\text{acc}})^{\mu}}, \quad (19)$$

where m_{acc} and V_{acc} are the subhalo mass and maximum circular velocity at the time of accretion. In order to constrain the two free parameters ν and μ , we use results from the Rhapsody simulation project (Wu et al. 2013a,b), a large suite of 96 high-resolution, simulations of cluster-sized dark matter haloes with a present-day mass of $M = 10^{14.8 \pm 0.05} h^{-1} \text{ M}_{\odot}$. These have been re-simulated with high resolution from a cosmological volume of $1 h^{-3} \text{ Gpc}^3$ in a ΛCDM cosmology with $\Omega_{\text{m}} = 0.25$, $\Omega_{\Lambda} = 0.75$, $\Omega_{\text{b}} = 0.04$, $h = 0.7$, $\sigma_8 = 0.8$ and spectral index $n_{\text{s}} = 1.0$ (hereafter ‘Rhapsody cosmology’). As in our model, the host haloes are defined as spherical, overdense regions with an average density equal to $\Delta_{\text{vir}} \rho_{\text{crit}}$. Using the 6D phase-space halo finder ROCKSTAR (Behroozi et al. 2013a,b), Wu et al. (2013b) measured subhalo mass and velocity functions covering more than four orders of magnitude in subhalo mass. Fig. 3 plots the ratio V_{\max}/V_{acc} as function of m/m_{acc} for a random subset of 2735 subhaloes from the Rhapsody simulations, kindly provided to us in electronic format by H. Wu. Fitting Eq. (19) to these data we obtain the best-fit relation indi-

cated by the red curve, which has $(\nu, \mu) = (0.44, 0.60)$. As we show in Paper II, the same relation also accurately fits results from the Bolshoi (Klypin et al. 2011) and MultiDark (Prada et al. 2012; Riebe et al. 2013) simulations, and is independent of host halo mass. For comparison, the solid and dashed blue curves are the $V_{\max}/V_{\text{acc}} - m/m_{\text{acc}}$ relations obtained by Peñarrubia et al. (2010) and Hayashi et al. (2003), respectively, using high-resolution, idealized N -body simulations of individual subhaloes orbiting in a static, spherical NFW host halo. These roughly bracket the results from the cosmological Rhapsody simulations.

2.4 Computing Subhalo Mass and Velocity Functions

Having described all the ingredients, we now outline how these are combined to compute the subhalo mass and velocity functions of a host halo of mass M_0 at redshift z_0 . We first construct a merger tree, with a mass resolution of $\psi_{\text{res}} = 10^{-5}$, as described in §2.1. Next, we follow each trajectory forward in time, starting from the redshift z_{acc} at which the trajectory’s halo first becomes a subhalo, evolving the subhalo mass in between merger-tree time steps all the way to $z = z_0$. The subhalo mass loss rate is given by Eqs. (1) - (2) with $\zeta = 0.07$, and a normalization \mathcal{A} that is a trajectory-specific random variable drawn from the following log-normal distribution

$$\mathcal{P}(\mathcal{A}) d\mathcal{A} = \frac{\log e}{\sqrt{2\pi} \sigma_{\log \mathcal{A}}} \exp \left[-\frac{\log^2(\mathcal{A}/\bar{\mathcal{A}})}{2 \sigma_{\log \mathcal{A}}^2} \right] \frac{d\mathcal{A}}{\mathcal{A}}. \quad (20)$$

Here $\sigma_{\log \mathcal{A}} = \sigma_{\log(\dot{m}/M)} = 0.17$ and the median $\bar{\mathcal{A}}$ is our model’s single free parameter, which we tune to reproduce the $z = 0$ subhalo mass function from simulations as described in §3.1 below. Note that this scatter in the normalization \mathcal{A} takes account of the scatter in subhalo mass loss rates due to the variance in orbital properties and halo concentrations.

Note that we loop over trajectories sorted by increasing order, which assures that each subhalo is evolved in its properly evolved parent halo. Throughout we also assume that subhaloes always continue to orbit within the parent halo that directly hosts it: in particular, if a first-order subhalo of mass m_1 is orbiting within a zeroth-order parent halo of mass m_0 , and hosts a second-order subhalo (i.e., a sub-subhalo) of mass m_2 , the latter is evolved using Eq (1) with $M = m_1$ and $m = m_2$, while m_1 is evolved using the same equation but with $M = m_0$ and $m = m_1$. In other words, we ignore the possibility that a higher-order subhalo is stripped from its direct parent, which would cause its order to decrease by one. We also ignore the possibility of subhalo-subhalo mergers inside a parent halo, which would cause the order of the less-massive subhalo to increase by one. As discussed in Paper II, these oversimplified assumptions do not seem to have a significant impact on the accuracy of our model.

In order to compute the subhalo velocity function, $dN/d \log(V_{\max}/V_{\text{vir}})$, with V_{vir} the virial velocity of the host halo, we compute V_{\max} at each time step along each trajectory of the host halo’s merger tree using the following approach. Starting from the trajectory’s leave point, we first use the P08 algorithm to construct the mass accretion his-

tory (MAH) back in time until the leaf’s most massive progenitor reaches a mass $M < 0.04 M_{\text{leaf}}$. This ‘extension’ of the merger tree is used to compute $t_{0.04}$ (using simple linear interpolation in between time steps), which is used in turn to compute V_{\max} for the leaf halo using Eqs. (16) - (18). Tracing the trajectory forward in time, each time step we use the past trajectory (plus its extension) to compute V_{\max} using the same approach. Once the halo associated with the trajectory becomes a subhalo, it starts to experience mass loss, as described by Eq. (1), and we use Eq. (19) with $(\nu, \mu) = (0.44, 0.60)$ to compute the evolution of its maximum circular velocity. As we demonstrate in §3 below, this method yields SHVFs in excellent agreement with simulation results (see also Paper II).

3 RESULTS

Our model as described above yields, at each redshift, the evolved SHMF and SHVF for all orders of subhaloes. In this section, we tune the free parameter $\bar{\mathcal{A}}$, compare the resulting model predictions with a few simulation results, and discuss how the subhalo mass and velocity functions scale with halo mass and redshift.

3.1 Testing and Calibrating the Model

The symbols with errorbars in Fig. 4 are the evolved SHMFs of first-order subhaloes at $z_0 = 0$, obtained by G08 using a set of simulations for a flat Λ CDM cosmology with $\Omega_m = 0.3$, $\Omega_\Lambda = 0.7$, $\Omega_b = 0.04$, $h = H_0/(100 \text{ km s}^{-1} \text{ Mpc}^{-1}) = 0.7$ and with initial density fluctuations described by a scale-invariant power spectrum with normalization $\sigma_8 = 0.9$. Host haloes are defined as spheres with an average density equal to $\Delta_{\text{vir}} \rho_{\text{crit}}$, and their subhaloes are identified using the subhalo finder SURV[§] that was developed by Tormen et al. (2004) and G08. Results are shown for two mass bins: $\log[M_0/(h^{-1} \text{ M}_\odot)] \in [12.0, 12.5]$, for which the average is 12.23, and $\log[M_0/(h^{-1} \text{ M}_\odot)] \in [13.5, 14.0]$, for which the average is 13.72. These bins contain a total of 3349 and 127 host haloes, respectively. The error bars indicate the rms values of $dN/d \log(m/M_0)$ in the logarithmic m/M_0 -bins with the width of 0.2 dex and bin-centers corresponding to the positions of the symbols.

The solid curves in Fig. 4 are the corresponding model predictions for host haloes of mass $M_0 = 10^{12.23} h^{-1} \text{ M}_\odot$ and $M_0 = 10^{13.72} h^{-1} \text{ M}_\odot$, respectively, obtained by averaging over 10,000 Monte Carlo realizations (i.e., merger trees). We have tuned $\bar{\mathcal{A}}$, which basically controls the overall normalization, such that the model curves match the G08 simulation results. The resulting best-fit value is $\bar{\mathcal{A}} = 1.34$ (corresponding to a present-day mass-loss time scale of $\tau_0 = 2.3 \text{ Gyr}$). Interestingly, with $\bar{\mathcal{A}}$ close to unity, we have that the average time scale for subhalo mass loss is basically just the dynamical time of the halo. We return to this somewhat intriguing result in §5. From here on we keep $\bar{\mathcal{A}}$ fixed, so that the model is fully determined.

[§] SURV differs from most other subhalo finders in that it uses prior information based on the host halo’s merger tree to identify its subhaloes.

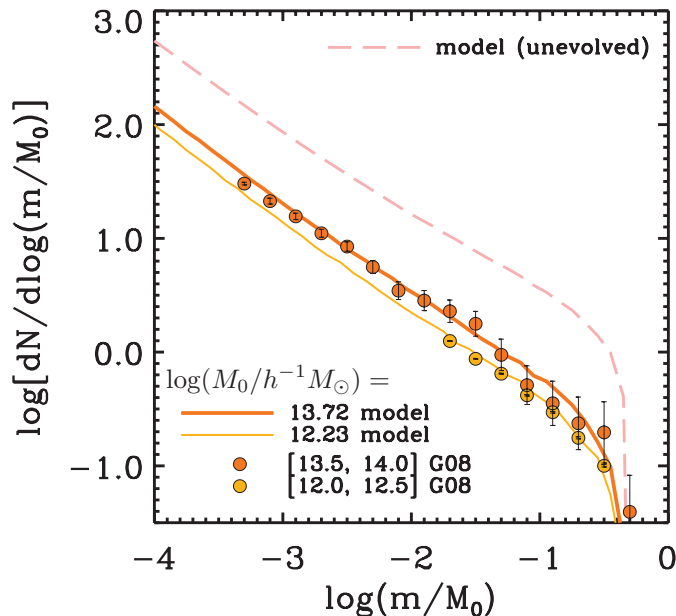


Figure 4. Comparison of average, evolved SHMFs at $z = 0$ obtained from N -body simulations (symbols with errorbars) with predictions from our semi-analytical model (solid lines). The simulation data is taken from the study by G08 and corresponds to host halo mass bins of $\log[M_0/(h^{-1}M_\odot)] \in [12.0, 12.5]$ and $[13.5, 14.0]$, as indicated. The model results have been obtained averaging over 10,000 Monte Carlo realizations for host haloes of $M_0 = 10^{12.23} h^{-1} M_\odot$ and $10^{13.72} h^{-1} M_\odot$, which are the average halo masses in the corresponding mass bins from the simulation. Finally, the dashed curve is the unevolved subhalo mass function, obtained from our merger trees, and is shown for comparison.

Note that our best-fit value for $\bar{\mathcal{A}}$ is in good agreement with the $\bar{\mathcal{A}} = 1.54^{+0.52}_{-0.31}$ obtained by G08 from the median mass loss rates inferred directly from their simulations. This is a dramatic improvement with respect to B05, who inferred $\bar{\mathcal{A}} = 23.7$, and owes entirely to the use of more accurate merger trees. Note that our model accurately reproduces the slope and host mass dependence of SHMF (see also Paper II and §3.2 below), which is a feature that cannot be controlled by the freedom in $\bar{\mathcal{A}}$. It is worth mentioning that the stochasticity in the mass-loss model ($\sigma_{\log \mathcal{A}} = 0.17$) actually causes a boost of the normalization of the SHMF; if we ignore this stochasticity, the best-fit value for the median mass-loss normalization is $\bar{\mathcal{A}} \sim 1.2$. The fact that the best-fit value for $\bar{\mathcal{A}}$ depends on the (amount of) stochasticity used is a manifestation of the log-normal nature of the distribution of orbit-averaged mass loss rates (see right-hand panel of Fig. 2), which causes the mean to be larger than the median.

Finally, the dashed curve in Fig. 4 represents the *unevolved* SHMFs obtained from the same Monte Carlo merger trees. Note that the unevolved SHMF is independent of host halo mass (see e.g., B05; Li & Mo 2009; Yang et al. 2011), and is therefore identical for the two mass bins shown. The differences between this (universal) dashed curve and the solid curves reflects the global impact of subhalo mass stripping integrated over the assembly history of the host halo.

To further test our model, we once more use the Rhapsody simulations of Wu et al. (2013a,b). The filled circles in

Fig. 5 are the average, cumulative mass and velocity functions for subhaloes of all orders obtained by Wu et al., using the subhalo finder ROCKSTAR. Note that these are normalized with respect to the present day mass, M_0 , and virial velocity, $V_{\text{vir},0}$, of their host halo. Because of the high resolution of the Rhapsody simulations, the Wu et al. data probes subhaloes all the way down to $m = 10^{-5} M_0$ ($V_{\text{max}} \sim 0.03 V_{\text{vir},0}$), an improvement of ~ 1.5 orders of magnitude in normalized subhalo mass with respect to the G08 results shown in Fig. 4. However, at the massive end the results published by Wu et al. (2013b) only extent to $m \sim 0.03 M_0$ ($V_{\text{max}} \sim 0.3 V_{\text{vir},0}$), which is roughly where the cumulative abundances drop below unity. We therefore complement the data of Wu et al. (2013b) with simulation data from the MultiDark simulation, which covers a cosmological volume of $1 h^{-3} \text{Gpc}^3$, but at significantly lower resolution. Using the publicly available ROCKSTAR catalog[¶] of haloes and subhaloes at $z = 0$, we compute the cumulative SHMF and SHVF, averaged over 2393 host haloes with masses in the range $10^{14.5} h^{-1} M_\odot \leq M_0 \leq 10^{15} h^{-1} M_\odot$. The results are shown as open circles in Fig. 5, and cover the ranges $m/M_0 \gtrsim 10^{-3}$ and $V_{\text{max}}/V_{\text{vir},0} \gtrsim 0.15$. Note that the MultiDark and Rhapsody results are in excellent agreement in the range where they overlap. This is true despite the fact that the MultiDark simulation corresponds to a slightly different cosmology ($[\Omega_m, \Omega_\Lambda, \Omega_b, h, \sigma_8, n_s] = [0.27, 0.73, 0.047, 0.7, 0.82, 0.95]$) than the Rhapsody simulations. Using our semi-analytical model, we have verified though that this slight difference in cosmological parameters has a negligible impact on the SHMF (see Paper II).

The solid curves in Fig. 5 correspond to our model predictions, averaged over 10,000 Monte Carlo realizations of host haloes with a present-day mass of $M_0 = 10^{14.8} h^{-1} M_\odot$ in the Rhapsody cosmology. In order to estimate the SHMF and SHVF for subhaloes of all orders we have summed the contributions of orders one to four; as shown below, the contribution of subhaloes of even higher order is negligible (see also JB14). The grey bands indicate the standard deviation due to halo-to-halo variance, while the dashed curves reflect the *unevolved*, cumulative SHMF and SHVF. Note that our semi-analytical model accurately reproduces the simulation results over the entire ranges in m/M_0 and $V_{\text{max}}/V_{\text{vir},0}$ shown, without tuning any of the parameters in our mass loss model or in the P08 merger tree algorithm. Hence, we conclude that our model can accurately reproduce both the SHMFs and SHVFs for subhaloes of first order and all orders, and for different host halo masses and cosmologies. This conclusion is further strengthened in Paper II, where we compare our model predictions with an even larger set of simulation results.

3.2 Mass and Redshift Dependence

Having tested and calibrated our mass-loss model, we now explore how the subhalo mass and velocity functions scale with host halo mass, redshift and subhalo order. To that extent we compute the average SHMFs, $dN/d\log(m/M_0)$, and SHVFs, $dN/d\log(V_{\text{max}}/V_{\text{vir},0})$, averaged over 10,000 Monte Carlo realizations, for host haloes

[¶] <http://hipacc.ucsc.edu/Bolshoi/MergerTrees.html>

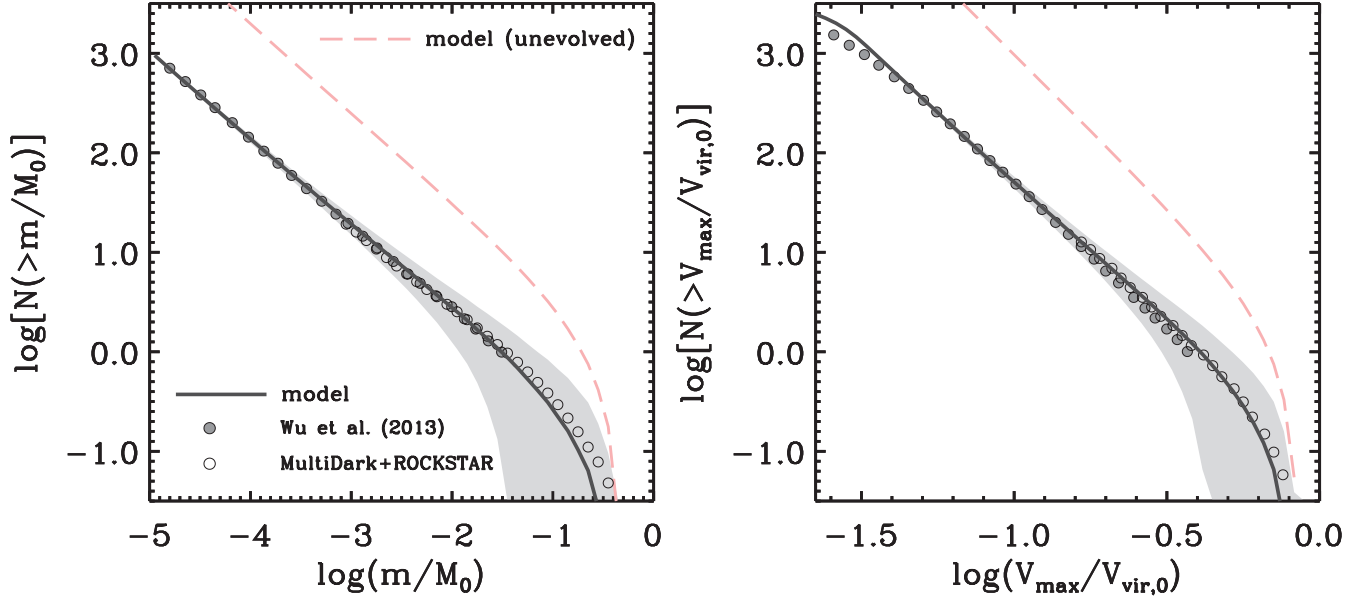


Figure 5. The average, cumulative mass function (left-hand panel) and velocity function (right-hand panel) at $z = 0$ for subhaloes of all orders in host haloes of mass $M_0 \simeq 10^{14.8} h^{-1} M_\odot$. The filled and open circles are results from the high-resolution Rhapsody simulations (Wu et al. 2013b; $M_0 = 10^{14.8 \pm 0.05} h^{-1} M_\odot$) and the publicly available MultiDark simulation (Prada et al. 2012; $M_0 \in [10^{14.5}, 10^{15}] h^{-1} M_\odot$), respectively, and have both been obtained using the (sub)halo finder ROCKSTAR. The solid curves are our model predictions for $M_0 = 10^{14.8} h^{-1} M_\odot$, averaged over 10,000 Monte Carlo realizations based on the Rhapsody cosmology. The gray bands indicate the corresponding halo-to-halo variance, while the dashed curves indicate the corresponding unevolved mass and velocity functions. Note the exquisite agreement between model and simulation results.

of masses $\log[M_0/(h^{-1} M_\odot)] = 11, 12, \dots, 15$, and redshifts $z_0 = 0, 1, 3$ and 5 in the Rhapsody cosmology.

The upper, left-hand panel of Fig. 6 plots the $z = 0$ SHMFs for the five different host halo masses, as indicated. Solid and dashed curves correspond to evolved and unevolved SHMFs. As already mentioned several times, the latter is universal, and therefore displays no mass dependence. The evolved SHMFs on the other hand, are clearly mass-dependent with a normalization that increases systematically with increasing host halo mass. This mass dependence, first noticed in numerical simulations by Gao et al. (2004) and in semi-analytical models by B05, simply reflects that more massive haloes form later: the universality of the unevolved SHMF shows that, on average, all haloes accrete (sub)haloes of the same, normalized mass. Since subhaloes that are accreted earlier will be more depleted, host haloes that assemble earlier, accrete their subhaloes earlier, which thus will be more depleted by the present day.

The upper, middle panel of Fig. 6 plots the $z = 0$ SHMFs of different orders for a host halo of mass $M_0 = 10^{13} h^{-1} M_\odot$, as indicated. Note how with each increasing order the normalization reduces by roughly an order of magnitude, while the slope steepens. Hence, when computing the SHMF for subhaloes of all orders one only has to sum the contributions of subhaloes of orders one and two, unless one aims to reach exquisite precision. Throughout this paper we always sum subhaloes up to fourth order, but none of our results would change noticeably if we were to ignore the third and fourth order subhaloes. The gray line shows the SHMF of all orders, which is clearly completely dominated by first-order subhaloes. Note, though, that the slope of the SHMF

of all orders is slightly, but significantly, steeper than that of first-order subhaloes (see §4 below).

The upper, right-hand panel Fig. 6 plots the SHMFs of all orders for host haloes of mass $M_0 = M_0(z_0) = 10^{13} h^{-1} M_\odot$ at different redshifts z_0 as indicated. At higher redshifts host haloes of the same mass have a larger abundance of subhaloes than their counterparts at lower redshifts. The unevolved SHMF, on the other hand, is independent of redshift. As discussed in B05, the subhalo mass fraction of a given halo at redshift z is a trade-off between the time scale, τ_{acc} , on which new subhaloes are being ‘accreted’ by the host halo, and the time scale, $\tau = \tau_{\text{dyn}}/\mathcal{A} \simeq \tau_{\text{dyn}}$, of subhalo mass loss. The latter evolves with redshift as described by Eq. (2), and therefore was shorter in the past. The former depends on the detailed mass assembly history of the host halo, and is thus a function of both redshift and halo mass. In the limit where $\tau_{\text{acc}} \ll \tau_{\text{dyn}}$, subhalo mass loss is negligible and the normalization of the SHMF will increase with time. The opposite limit, in which $\tau_{\text{acc}} \gg \tau_{\text{dyn}}$, is equivalent to that of subhalo mass loss in a static parent halo. In this case, the normalization of the SHMF will decrease with time. Since τ_{acc} is of order the Hubble time, which is always larger than the dynamical time of a halo, we are in the latter regime, which explains why the normalization of the SHMF decreases with decreasing redshift.

The lower panels of Fig. 6 plot the same results as the upper panels, but for the SHVFs. Overall the trends are very similar except for one important difference: the unevolved SHVFs are *not* universal. As is evident from the lower left- and lower right-hand panels, the unevolved SHVF increases with decreasing host halo mass and decreasing redshift. As discussed in §4 below, this is a consequence of the

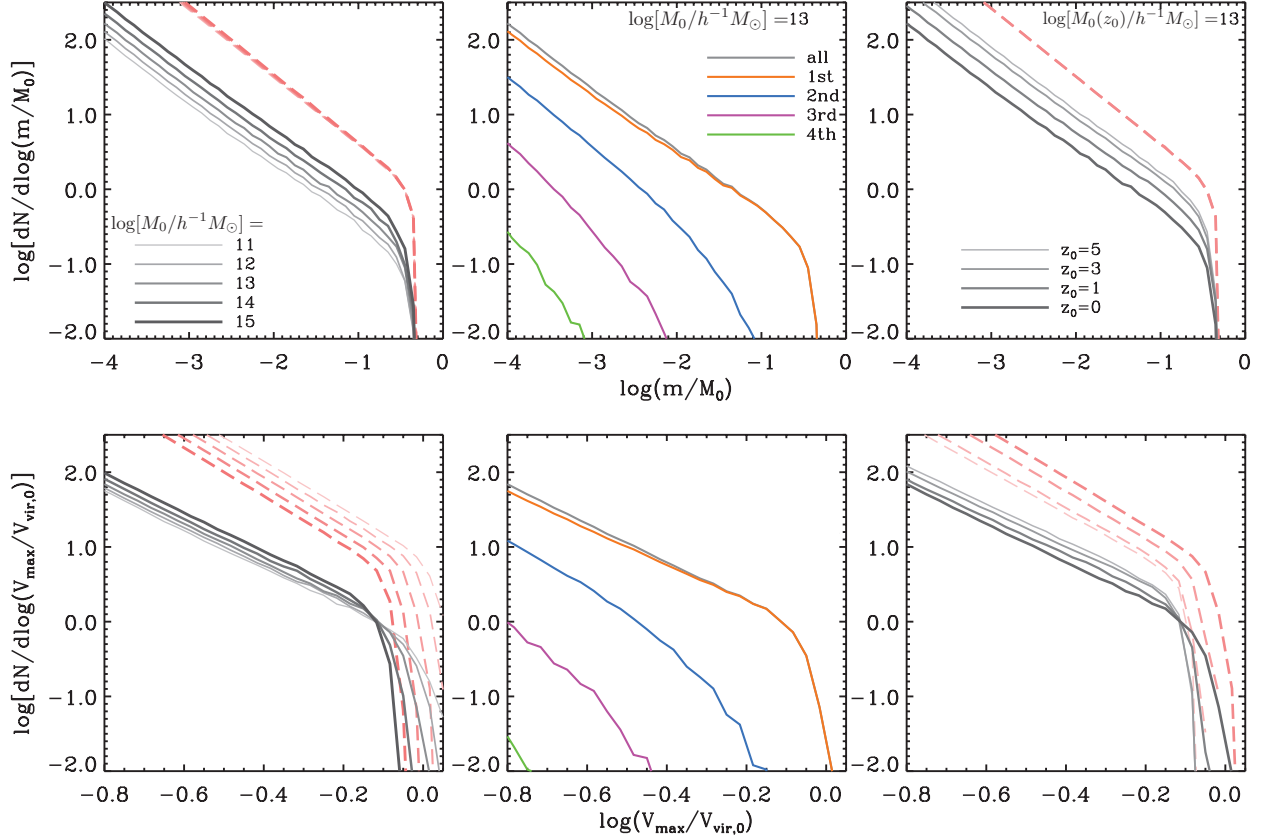


Figure 6. Average SHMFs (upper panels) and SHVFs (lower panels) obtained by averaging over 10,000 merger trees each. *Left-hand panels:* Results for different host halo masses, as indicated, with solid and dashed curves corresponding to the evolved and unevolved mass/velocity functions, respectively. *Middle panels:* Evolved SHMFs and SHVFs of different orders (different colors, as indicated), for a host halo of mass $M_0 = 10^{13} h^{-1} M_\odot$ at $z = 0$. *Right-hand panels:* Results for a host halo of mass $M_0 = 10^{13} h^{-1} M_\odot$ at different redshifts, as indicated. As in the left-hand panels, solid and dashed curves correspond to evolved and unevolved mass/velocity functions, respectively. Note how the unevolved SHMF is independent of mass and redshift, which is not the case for the unevolved SHVF.

concentration-mass-redshift relation of dark matter haloes, and causes a cross-over in the mass- and redshift- dependence of the evolved SHVFs at the massive end.

4 UNIVERSAL MODELS FOR THE SUBHALO MASS AND VELOCITY FUNCTIONS

Fig. 6 suggests that the SHMF has a universal shape, with a normalization that depends on halo formation time. This universality has its origin in the universal shape of the *unevolved* SHMF, and suggest that it should be straightforward to obtain a fitting function for the *evolved* SHMF, $dN/d\ln(m/M_0)$, that is valid for any M_0 , any redshift, z_0 , and any cosmology. In fact, the results of Fig. 6 suggest that a similar universal fitting function may be found for both the evolved and unevolved SHVFs. In this section we present such universal fitting functions, and demonstrate how their normalizations can be computed from very simple considerations. The results of this section are summarized in Appendix A, where we provide a simple step-by-step description of how to compute these universal fitting functions.

Before we proceed, though, we caution that what follows should only be used to describe subhalo mass and velocity functions in Λ CDM cosmologies with parameters that

are roughly consistent (within a factor ~ 2) with current constraints. The reason is that the alleged universality of the *unevolved* SHMF, first eluded to by B05 and then confirmed in numerical simulations by G08 and Li & Mo (2009), only holds approximately. This was demonstrated in Yang et al. (2011), who showed that the slope of the unevolved SHMF depends weakly, but significantly, on the effective slope of the matter power spectrum.

In order to have a sufficient dynamic range to probe how the subhalo mass and velocity functions scale with mass and cosmology, we construct average SHMFs and SHVFs for host haloes spanning the mass range $10^{11} h^{-1} M_\odot \leq M_0 \leq 10^{15} h^{-1} M_\odot$ in cosmologies that span the range $0.1 \leq \Omega_m \leq 0.5$, $0.5 \leq \sigma_8 \leq 1.0$ and $0.5 \leq h \leq 1.0$. Our ‘baseline’ is a host halo of mass $M_0 = 10^{13} h^{-1} M_\odot$ in the Rhapsody cosmology $[(\Omega_m, h, \sigma_8) = (0.25, 0.73, 0.8)]$, which falls roughly midway of the ranges considered. When varying cosmology, we only vary one of these three cosmological parameters per time with respect to this baseline cosmology and compute the average SHMF and SHVF for host haloes with $M_0 = 10^{11} h^{-1} M_\odot$ and $10^{15} h^{-1} M_\odot$, in each case averaging over 20,000 Monte Carlo realizations at redshift $z_0 = 0$.

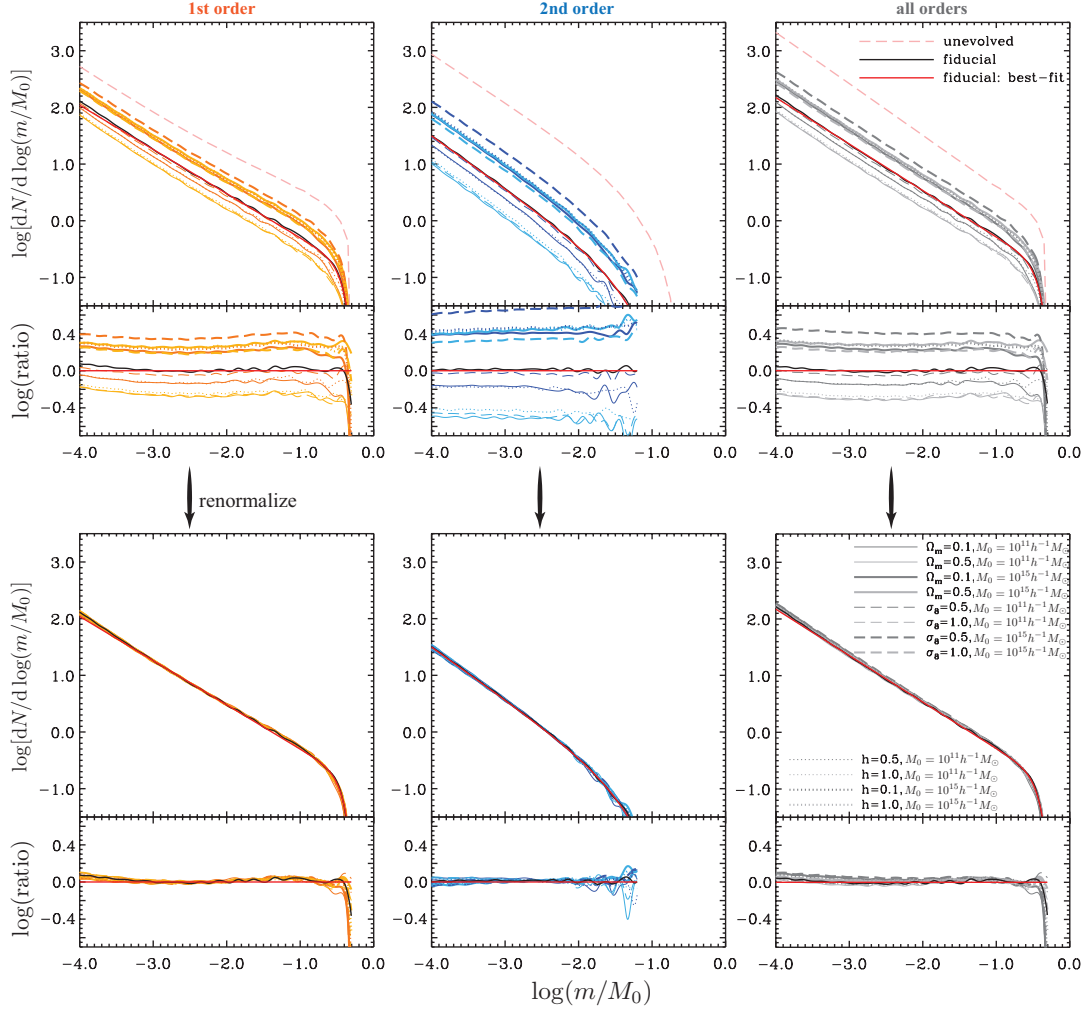


Figure 7. The average SHMFs at redshift $z = 0$ for different cosmologies and host halo masses obtained by averaging over 20,000 merger trees each. Panels in the upper and lower rows show the results before and after renormalization by the subhalo mass fraction f_s , as described in the text. Panels in the left, middle, and right columns show the results for subhaloes of first order, second order, and all orders. Curves of different line style and thickness correspond to different cosmology and halo mass, as indicated. The solid black curves represent the fiducial ‘baseline’ model, which corresponds to a host halo of mass $M_0 = 10^{13} h^{-1} M_\odot$ in the Rhapsody cosmology. The dashed, light-red curves in the upper panels of the upper row represent the universal *unevolved* SHMFs. Solid, red curves are the fitting functions of the form of Eq. (22) that best-fit the fiducial baseline model; the bottom panels in each row show the ratios with respect to this fitting function.

4.1 Evolved Subhalo Mass Function

The upper panels of Fig.7 plot the SHMFs for $z = 0$ host haloes with masses of $10^{11} h^{-1} M_\odot$ and $10^{15} h^{-1} M_\odot$ for the 6 extreme cosmologies considered here. The left, middle, and right columns show the results for first-order subhaloes, second-order subhaloes, and subhaloes of all-orders, respectively. The dashed, light-red curves are the corresponding unevolved SHMFs, which are virtually identical for all masses and cosmologies shown. As expected, the evolved SHMFs also have very similar shapes, but normalizations that differ by up to ~ 1.1 dex. Upon inspection, one can discern that the normalization of the evolved SHMF increases with increasing Ω_m and M_0 , and with decreasing h and σ_8 .

The normalization of the SHMF can be characterized by the total mass fraction in subhaloes with masses $m \geq \psi_{\text{res}} M_0$:

$$f_s \equiv \int_{\psi_{\text{res}}}^1 \psi \frac{dN}{d\psi} d\psi = \int_{\psi_{\text{res}}}^1 \frac{dN}{d \ln \psi} d\psi, \quad (21)$$

where we have used ψ as shorthand for m/M_0 . Throughout this section we adopt a mass resolution of $\psi_{\text{res}} = 10^{-4}$. In the lower panels of Fig. 7, we have renormalized the SHMFs in the upper panels by multiplying $dN/d \log(m/M_0)$ with the factor $f_{s,\text{fid}}/f_s$, where $f_{s,\text{fid}}$ is the subhalo mass fraction of our fiducial ‘baseline’ (i.e., a host halo of mass $M_0 = 10^{13} h^{-1} M_\odot$ in the Rhapsody cosmology). Clearly, this renormalization brings all SHMFs in excellent agreement with each other; the small discrepancies at the massive end are consistent with being due to statistical noise. Hence, we conclude that the evolved SHMFs (of any given order) constitute a universal, one-parameter family.

This family of functions can be well fitted by a Schechter-like function of the form

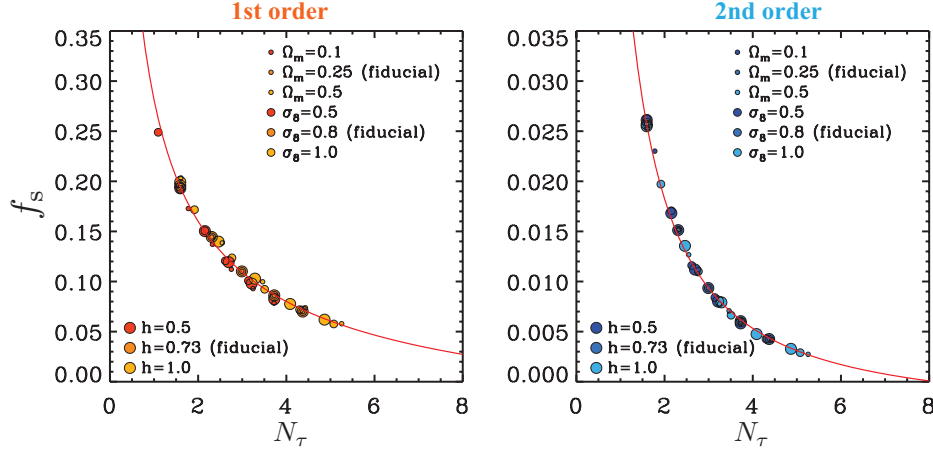


Figure 8. The relation between subhalo mass fraction f_s and the host halo’s ‘dynamical age’, N_τ , defined as the number of dynamical time scales elapsed, since the formation of the (average) host halo (see Eq. [24]). The left- and right-hand panels correspond to first- and second-order subhaloes, respectively. Filled circles of different colors and sizes represent different cosmologies and host halo masses, as indicated, while the solid, red lines are the best-fit relations of Eqs. (26) and (27).

$$\frac{dN}{d \ln \psi} = \gamma \psi^\alpha \exp(-\beta \psi^\omega), \quad (22)$$

where α , β , γ and ω are free parameters. The best-fit values for the power-law slope α are -0.78 , -0.93 , and -0.82 for the SHMFs of first-order, second-order and all-orders, respectively. Note that studies of subhalo mass functions based on N -body simulations have reported values for α for the SHMFs of all-orders that cover the entire range from -0.7 to -1.1 . As discussed in detail in Paper II, this large range owes partially to limited quality of the simulation data, but also to the fact that different studies have used different subhalo finders. The best-fit parameters for β and ω are somewhat degenerate, but we obtain good fits for $(\beta, \omega) = (50, 4)$ for SHMFs of first-order and all-orders and $(25, 1)$ for second-order subhaloes. Finally, the normalization constant γ is related to the subhalo mass fraction, f_s , via:

$$\gamma = \frac{\omega \beta^s}{\Gamma[s, \beta \psi_{\text{res}}^\omega] - \Gamma[s, \beta]} f_s, \quad (23)$$

with $\Gamma(a, x)$ the incomplete gamma function, and $s \equiv (1 + \alpha)/\omega$. The red, solid curves in Fig. 7 represent these best-fit functions to the fiducial ‘baseline’ SHMF, while the smaller panels show the ratios with respect to this fiducial fitting function. These reveal a very weak, but systematic, upturn at the low-mass end for SHMFs of first-order and all-orders. This upturn is not captured by the simple power-law behavior of Eq. (22). A similar, albeit more pronounced upturn, is also present in the *unevolved*, first-order SHMF, which, as shown by JB14, is therefore better described by a double-Schechter-like function, $dN/d \ln \psi = (\gamma_1 \psi^{\alpha_1} + \gamma_2 \psi^{\alpha_2}) \exp(-\beta \psi^\omega)$. Although the extra degrees of freedom of such a fitting function would also improve the quality of the fits to our inferred SHMFs, we don’t believe this is warranted by the level of accuracy of our model. We therefore choose to describe the evolved SHMFs with the simpler Eq. (22).

With the parameters α , β and ω specified, what remains is to obtain an easy-to-use characterization of the normalization parameter γ , or equivalently, of the subhalo mass fraction, f_s . The fraction of a halo’s mass that is locked up

in substructure is the outcome of a competition between halo accretion and halo stripping. For any particular subhalo, the mass that remains bound is basically determined by how long it has been exposed to tidal stripping. Since the *unevolved* SHMF is universal, it is therefore natural to suspect that the subhalo mass fraction, f_s , of a host halo is closely correlated to its ‘age’, expressed in units of the dynamical time. For a host halo of mass M_0 at redshift z_0 this can be defined as

$$N_\tau(M_0, z_0) \equiv \int_{t_0}^{t(z_{\text{form}})} \frac{dt}{\tau_{\text{dyn}}(t)}. \quad (24)$$

Here t is the lookback time, $\tau_{\text{dyn}}(t)$ is the corresponding dynamical time given by Eq. (2), t_0 is the lookback time to redshift z_0 , and $z_{\text{form}} = z_{\text{form}}(M_0, z_0)$ is the halo’s formation redshift, which we define as the redshift at which the main progenitor of the halo has reached a mass $M_0/2$. As we demonstrate below, formulating the age of the halo in terms of the elapsed number of dynamical times captures all the relevant mass, redshift and cosmology dependence.

In order to compute the formation redshift, z_{form} , we use the model of Giocoli et al. (2012; hereafter G12), which yields, for any cosmology, the median redshift z_f at which the main progenitor of a halo of mass M_0 at redshift z_0 has reached a mass fM_0 . This requires solving

$$\delta_c(z_f) = \delta_c(z_0) + \tilde{w}_f \sqrt{\sigma^2(fM_0) - \sigma^2(M_0)}, \quad (25)$$

where $\tilde{w}_f = \sqrt{2 \ln(\alpha_f + 1)}$ and $\alpha_f = 0.815 e^{-2f^3} / f^{0.707}$. Here $\sigma^2(M)$ is the mass variance and $\delta_c(z) \equiv 1.686/D(z)$ with $D(z)$ the linear growth rate normalized to unity at $z = 0$. We define z_{form} as the solution of Eq. (25) for z_f with $f = 0.5$.

Fig. 8 plots the subhalo mass fraction, f_s , obtained from the evolved SHMFs shown in Fig. 7, as function of the halo ‘age’ N_τ , computed using Eq. (24) with z_{form} obtained from the G12 model as described above. As expected, these two quantities are tightly correlated. We find that the subhalo mass fractions for first and second order subhaloes are accurately described by

$$f_{s,1st} = \frac{0.3563}{N_\tau^{0.6}} - 0.075, \quad (26)$$

and

$$f_{s,2nd} = \frac{0.0535}{N_\tau^{1.3}} - 0.0035, \quad (27)$$

respectively, which are indicated by the red lines. We emphasize that these relations are valid for any halo mass, M_0 , any redshift, z_0 , and any reasonable Λ CDM cosmology. Note that, since our halo mass definition is ‘inclusive’, the first-order mass fraction $f_{s,1st}$ also describes the mass fraction in subhaloes of all orders. Also, recall that the mass fractions in Eqs. (26) and (27) correspond to a mass resolution of $\psi_{res} = 10^{-4}$. This needs to be taken into account when using these mass fractions to compute the SHMF normalization parameter, γ , with the help of Eq. (23).

The above relations between f_s and N_τ allow one to write down the average, evolved SHMF for a halo of arbitrary mass, at any redshift, and for a wide range of Λ CDM cosmologies. We now examine whether similar, universal fitting functions can be found to describe both the evolved and unevolved SHVFs.

4.2 The Unevolved SHVF

The unevolved SHVF, $dN/d\ln(V_{acc}/V_{vir,0})$, provides the basis for the popular technique of subhalo abundance matching. Unfortunately, the convenient universality present in the case of the unevolved mass function does not hold for the unevolved velocity function. This is easy to understand from the fact that the relation between m_{acc} and $V_{acc} = V_{max}(z_{acc})$ depends on the concentration-mass-redshift relation. Hence, the ‘mapping’ of m_{acc}/M_0 into $V_{acc}/V_{vir,0}$ depends on mass, redshift and cosmology.

The left-hand panels of Fig. 9 show the unevolved SHVFs of all-orders for host haloes of different masses in the Rhapsody cosmology, as indicated. These have been obtained averaging over 20,000 Monte-Carlo realizations. Although both the normalization and the scale at which the transition to exponential decay occurs differ from one SHVF to the other, the shapes still look close to universal. Hence, it is natural to describe the unevolved velocity function with a functional form

$$\frac{dN}{d\ln\psi} = \gamma (a\psi)^\alpha \exp[-\beta(a\psi)^\omega], \quad (28)$$

where we have introduced a scale parameter, a , in addition to the free parameters α , β , γ , and ω . We now seek to find a parameterization of a for which the unevolved SHVF is (close to) universal, i.e., for which the other parameters are independent of host mass, redshift and cosmology.

To do so, we use the fact that

$$\frac{V_{max}(m_{acc}, z_{acc})}{V_{vir}(M_0, z_0)} = \frac{V_{max}(m_{acc}, z_{acc})}{V_{vir}(m_{acc}, z_0)} \times \frac{V_{vir}(m_{acc}, z_0)}{V_{vir}(M_0, z_0)}. \quad (29)$$

Since the second factor on the right-hand side only depends on m_{acc}/M_0 , and has no dependence on cosmology or redshift, and since the mass function of m_{acc}/M_0 is universal, a logical choice for the scale factor a is $V_{vir}(\langle m_{acc} \rangle, z_0)/V_{max}(\langle m_{acc} \rangle, \langle z_{acc} \rangle)$ where $\langle m_{acc} \rangle$ and $\langle z_{acc} \rangle$ are representative values for the mass and redshift at accretion. For the latter we use the redshift z_f by which the main progenitor of the host halo has assembled a fraction f of

its final mass M_0 . For the characteristic subhalo mass at accretion we take $\langle m_{acc} \rangle = M_0/10$, which is close to the exponential cut-off scale of the unevolved SHMF. Hence, we have that

$$a = C \frac{V_{vir}(0.1fM_0, z_0)}{V_{max}(0.1fM_0, z_f)}, \quad (30)$$

where we have introduced the normalization C which we tune such that $a = 1$ for our fiducial ‘baseline’ model. For a given value of f , one can use the G12 model to compute the corresponding z_f , and use Eqs. (17) and (16) to compute $V_{vir}(0.1fM_0, z_0)$ and $V_{max}(0.1fM_0, z_f)$, respectively. The latter requires the halo concentration parameter, c , which we compute using the concentration-mass-redshift relation of Zhao et al. (2009).

We have experimented with different values for f , and obtain the best results for $f = 0.25$, for which $C = 1.536$. The right-hand panels of Fig. 9 plot $dN/d\log(V_{acc}/V_{vir,0})$ versus $aV_{acc}/V_{vir,0}$, where a is computed using Eq. (30) with these best-fit values. It is clear that this simple rescaling accounts for virtually all the halo mass dependence in the unevolved SHVF. The rescaled, unevolved SHVFs are almost indistinguishable from each other and are well fit by Eq. (28) with $\alpha = -3.2$, $\beta = 2.2$, $\gamma = 2.05$, $\omega = 13$, and $a = 1$ (red curve). Some discrepancies that go beyond statistical noise are evident at the high-velocity end ($aV_{acc}/V_{vir,0} \gtrsim 0.9$), but only for the most massive host haloes. Although the discrepancies are within a factor of two, we caution that the ‘universal’ unevolved SHMF presented here is less reliable for the most massive subhaloes in the most massive (cluster-sized) host haloes.

We have also verified that the same scale parameter a (with $f = 0.25$) also describes the cosmology- and redshift- dependences quite well. There is a weak dependence of the power-law slope α on cosmology, but this only becomes cumbersome when the cosmological parameters deviate substantially (i.e., by about a factor of two or more) from the ‘baseline’ Rhapsody cosmology with $(\Omega_m, h, \sigma_8) = (0.25, 0.73, 0.8)$. Overall, though, the rescaling introduced here, and summarized in Appendix A, allows one to compute reliable, unevolved subhalo velocity functions for host haloes of different mass, at different redshifts, and for a broad range of Λ CDM cosmologies.

4.3 The Evolved SHVF

The left-hand panels of Fig. 10 plot the *evolved* SHVFs corresponding to the *unevolved* SHVFs shown in Fig. 9. Similar to the evolved *mass* functions, the power-law slopes of the evolved *velocity* functions are independent of host halo mass, and the normalization increases with increasing M_0 . However, at the high-velocity end this halo mass-dependence flips over, and the exponential cut-off occurs at smaller $V_{max}/V_{vir,0}$ for more massive host haloes. As we demonstrate in Paper II, these trends are consistent with results from N -body simulations.

In an attempt to construct a universal fitting function for the *evolved* SHVF, we first apply the rescaling that successfully describes the non-universality of the *unevolved* SHVF. This results in the rescaled velocity functions shown in the middle panels of Fig. 10. The cut-off now occurs at roughly the same scale, which has removed the ‘cross-over’

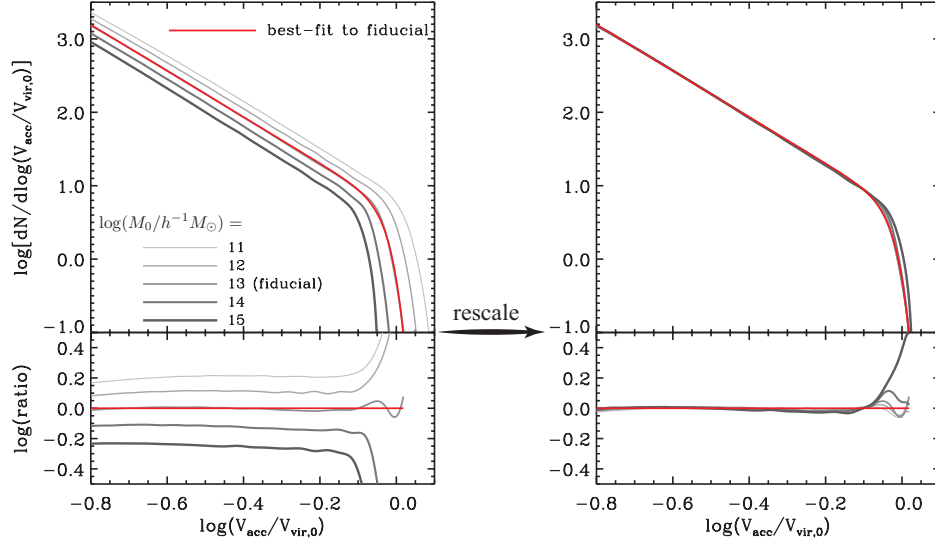


Figure 9. Panels on the left show the unevolved subhalo velocity functions, $dN/d\log(V_{\text{acc}}/V_{\text{vir},0})$, for five different host halo masses, as indicated, in the Rhapsody cosmology. Each of these has been obtained by averaging 20,000 merger trees. In the panels on the right, these have been rescaled using the scale parameter a given by Eq. (30). In both panels the red curves correspond to the fitting function of the form of Eq. (28) that best-fit the results for $M_0 = 10^{13} h^{-1} M_\odot$, which has best-fit parameters $\alpha = -3.2$, $\beta = 2.2$, $\gamma = 2.05$, $\omega = 13$, and (by definition) $a = 1$. The bottom panel plots the ratios relative to this fitting function.

present in the left-hand panels. The normalizations, though, still depend on host halo mass, which reflects the impact of subhalo mass evolution. Hence, we expect that this normalization scales with the halo’s dynamical age, N_τ . Recall that in the case of the evolved mass function, the normalization constant is simply proportional to the subhalo mass fraction f_s , which, after all, is simply an integral of the mass function. In the case of the evolved SHVF, we assume that the normalization scales with f_s^b , where b is some constant. By trial and error we find that $b = 1.4$ accurately captures the scaling of the SHVFs. This is demonstrated in the right-hand panels of Fig. 10, which indicates that renormalization by $f_s^{1.4}$ yields SHVFs that are almost indistinguishable. This universal, evolved SHVF is well described by Eq. (28) with $(\alpha, \beta, \gamma, \omega) = (-2.6, 4, 0.248, 15)$. As with the *unevolved* SHVF, small discrepancies are evident at the high-velocity end for the most massive host haloes, but overall this two-stage process of rescaling and renormalization nicely captures the mass-, redshift- and cosmology dependence of the evolved SHVF for subhaloes of all-orders (see also Appendix A).

5 DISCUSSION

The results presented in this paper show that the orbit-averaged subhalo mass-loss rates are accurately described by

$$\dot{m} = -\mathcal{A} \frac{m}{\tau_{\text{dyn}}} \left(\frac{m}{M} \right)^\zeta. \quad (31)$$

with τ_{dyn} the halo’s (instantaneous) dynamical time, $\zeta = 0.07$, and \mathcal{A} a random variable that follows a log-normal distribution with median $\bar{\mathcal{A}} = 1.34$ and dispersion $\sigma_{\log \mathcal{A}} = 0.17$. This implies that, in an orbit-averaged sense, dark matter subhaloes evolve as

$$m(t) = m_{\text{acc}} \left[1 + \zeta \mathcal{A} \left(\frac{m_a}{M_0} \right)^\zeta \{ \tilde{N}_\tau(t_{\text{acc}}) - \tilde{N}_\tau(t) \} \right]^{-1/\zeta} \quad (32)$$

where t is *lookback time*, t_{acc} and m_{acc} are the lookback time and subhalo mass at accretion, M_0 is the present day mass of the host halo, and

$$\tilde{N}_\tau(t) \equiv \int_0^t \left[\frac{M(t)}{M_0} \right]^{-\zeta} \frac{dt}{\tau_{\text{dyn}}(t)} \quad (33)$$

is some measure for the number of dynamical times that have elapsed in an evolving dark matter halo since lookback time t .

It is interesting to see what this implies for the amount of mass that is stripped from a typical subhalo during its first radial orbit. In units of the mass of the subhalo at infall, this is given by

$$\frac{\Delta m}{m_{\text{acc}}} \equiv \frac{m_{\text{acc}} - m(t_{\text{acc}} - T_r)}{m_{\text{acc}}} \quad (34)$$

with T_r the radial orbital period given by Eq. (9). Without loosing generality, we set $t_{\text{acc}} = T_r$, so that the subhalo has just completed its first radial orbit at the present day. In this case, we have that

$$\frac{\Delta m}{m_{\text{acc}}} = 1 - \left[1 + \zeta \mathcal{A} \left(\frac{m_a}{M_0} \right)^\zeta \tilde{N}_\tau(T_r) \right]^{-1/\zeta} \quad (35)$$

Using the toy model described in §2.2.1 we find that the distribution of T_r at $z = 0$ is close to uniform over the interval [5, 9] Gyr, which has its origin in the uniform distribution of R_s (T_r depends strongly on E but has very little dependence on L).

The left-hand panel of Fig. 11 plots \tilde{N}_τ as function of lookback time, t , where we have assumed, for simplicity, that dark matter haloes grow in mass exponentially on a time scale τ_M , i.e., $M(t) = M_0 \exp(-t/\tau_M)$. We also assumed a ‘Planck cosmology’ with $\Omega_m = 0.318$, $\Omega_\Lambda = 0.682$

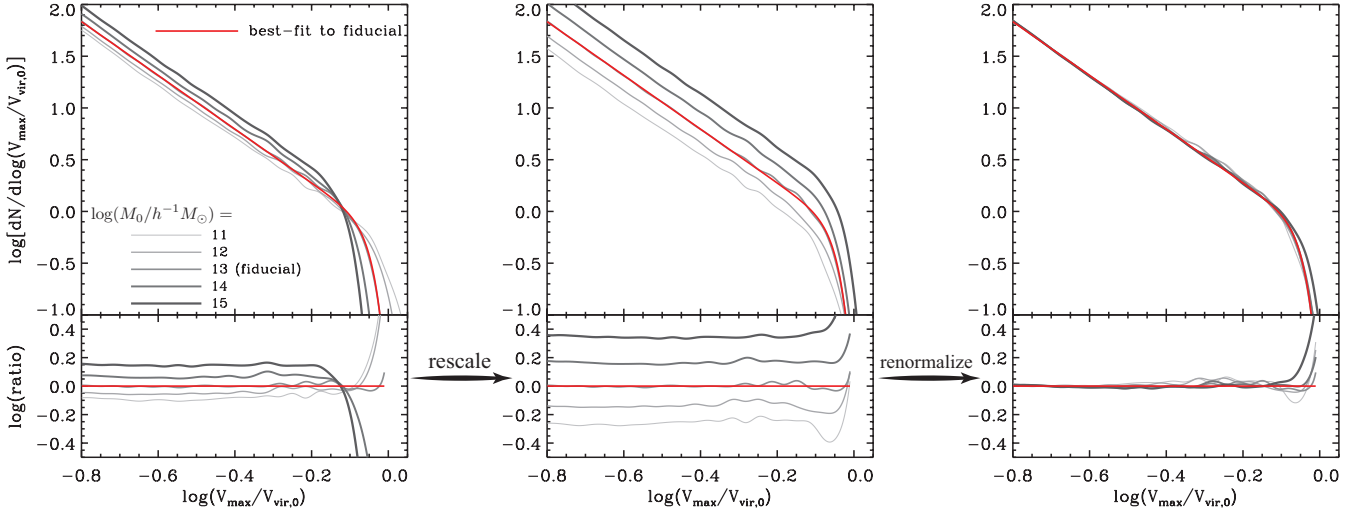


Figure 10. Same as Fig. 9, but here we show the corresponding results for the *evolved* SHVFs, $dN/d\log(V_{\max}/V_{\text{vir},0})$. After rescaling with the scale parameter a , the various SHVFs have a universal shape, but different normalizations (panels in middle column). This dependence can be renormalized by scaling the SHVFs with a factor $f_s^{1.4}$ (panels in right-hand column). After this two-step process of rescaling and renormalization, the evolved SHVFs are accurately described by Eq. (28) with $\alpha = -2.6$, $\beta = 4$, $\gamma = 0.248$, and $\omega = 15$ (red curves).

and $h = 0.671$, but we emphasize that the results are almost indistinguishable for other, similar cosmologies, such as those advocated by different data releases of the WMAP experiment. Results are shown for four different values of τ_M , ranging from infinity (i.e., no evolution in host halo mass) to $\tau_M = 1\text{Gyr}$ (i.e., host halo mass has grown by almost a factor three during the last Gyr). This more than covers the range of growth rates of dark matter haloes in the mass range $10^{11} h^{-1}M_\odot < M_0 < 10^{15} h^{-1}M_\odot$. As is evident, the interval $T_r \in [5, 9]\text{Gyr}$ translates roughly into $\tilde{N}_r(T_r) \in [2, 4]$, with very little dependence on τ_M ^{||}. Hence, the typical radial orbital period of a subhalo following infall lasts roughly 2 to 4 dynamical times. This may sound somewhat counter-intuitive, but note that the dynamical time is an average for the entire halo, which is not representative of orbits at first infall.

The right-hand panel of Fig. 11 plots the distribution of $\Delta m/m_{\text{acc}}$ for the same Planck cosmology, obtained using Eq. (35) with $\zeta = 0.07$ and $\tau_M = 10\text{Gyr}$ (roughly representative for a Milky-Way sized dark matter halo, though the results only depend very weakly on τ_M). The orbital periods, T_r , are sampled from a uniform distribution covering the range from 5 to 9 Gyr, while the mass-loss rate normalization parameter, \mathcal{A} , is sampled from the log-normal given by Eq. (20) with $\bar{\mathcal{A}} = 1.34$. Results are shown for five different values of m_{acc}/M_0 , as indicated. The medians of the distributions are indicated by arrows, and range from 0.80 for $m_{\text{acc}}/M_0 = 10^{-5}$ to 0.95 for $m_{\text{acc}}/M_0 = 10^{-1}$. Sampling m_{acc}/M_0 from the actual unevolved SHMF for $m_{\text{acc}}/M_0 \geq 10^{-5}$ yields a distribution that is intermediate between those for $m_{\text{acc}}/M_0 = 10^{-4}$ and $m_{\text{acc}}/M_0 = 10^{-5}$ with a median of 0.827. Note that only a minute fraction of subhaloes is expected to hang on to more than 50 percent of

their infall mass after one radial orbit. Hence, *subhaloes lose the vast majority (typically more than 80 percent) of their mass during their very first radial orbit*. We emphasize that most of this mass loss is likely to occur near pericenter (and hence, roughly a time $T_r/2$ after infall), but we caution that our model only treats orbit-averaged mass-loss rates, and should therefore not be used to make predictions regarding mass-loss rates on significantly shorter time-scales.

The dependence of $\Delta m/m_{\text{acc}}$ on m_{acc}/M_0 owes to two effects: (i) the concentration-mass relation of dark matter haloes, which makes subhaloes with a lower value of m_{acc}/M_0 relatively denser compared to its host halo, and therefore more resilient to tidal stripping, and (ii) dynamical friction, which will cause more massive subhaloes to lose more orbital energy and angular momentum, reducing their pericentric distance, and thus causing enhanced stripping. However, with the dramatic mass stripping rates revealed here, it is also clear that dynamical friction cannot play a very important role after first pericentric passage; as a rule of thumb, the dynamical friction time is only shorter than the Hubble time if $m/M \gtrsim 0.1$ (e.g., Mo, van den Bosch & White 2010). Even if a subhalo is that massive at infall, it is very likely to be stripped below this limit after its first pericentric passage. Hence, mass stripping is a far more important process for the evolution of dark matter subhaloes than dynamical friction (see also Taffoni et al. 2003; Taylor & Babul 2004; Peñarrubia & Benson 2005; Zentner et al. 2005; Gan et al. 2010), and one does not make large errors by ignoring dynamical friction altogether.

6 SUMMARY

We have presented a new semi-analytical model that uses EPS merger trees to generate evolved subhalo populations. The model is based on the method pioneered by B05, and evolves the mass of dark matter haloes using a simple model

^{||} This also implies that the results presented here are insensitive to deviations of $M(t)/M_0$ from an exponential

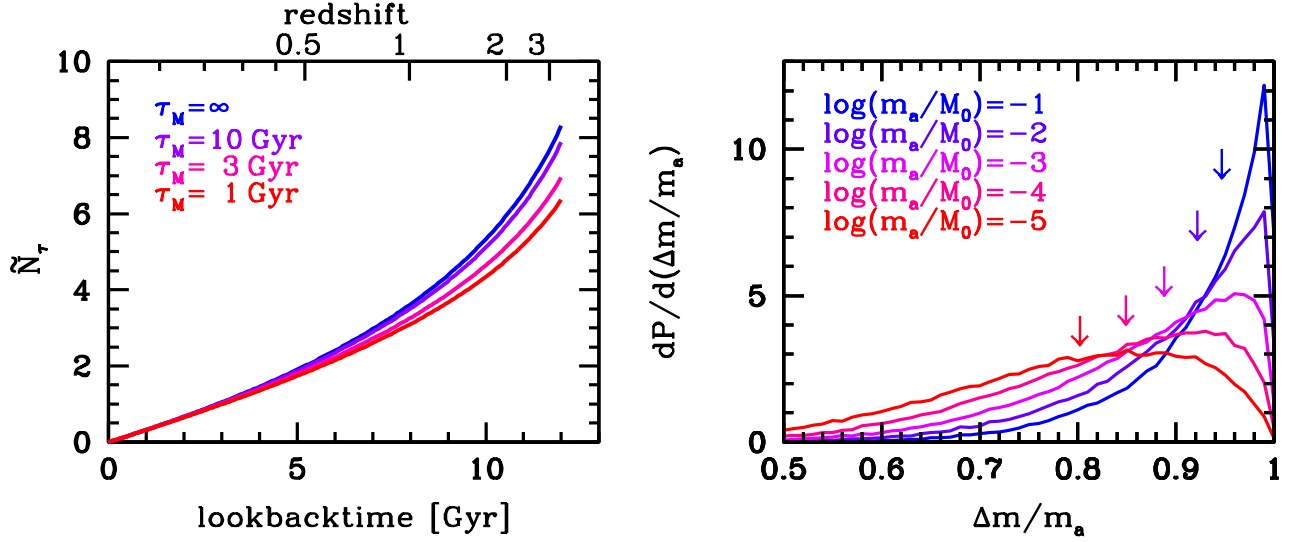


Figure 11. *Left-hand panel:* the quantity \tilde{N}_τ , defined by Eq. (33), as function of lookback time t for four different values of the time-scale for halo mass growth, τ_M , as indicated. As is apparent, \tilde{N}_τ is not very sensitive to how host halo masses grow over time. This is a manifestation of the small value for ζ , which indicates that subhalo mass loss rates depend only weakly on host halo mass. *Right-hand panel:* Distributions of the fractional subhalo mass lost during the first radial orbit after infall, $\Delta m/m_{\text{acc}}$. Results are shown for five different values of m_{acc}/M_0 , as indicated. Arrows indicate the medians of the corresponding distributions. Note that subhaloes, on average, lose more than 80 percent of their infall mass during their first radial orbit. All these results are for a Planck cosmology with $(\Omega_m, h) = (0.318, 0.671)$, but results are very similar for other Λ CDM cosmologies that are consistent with current observational constraints.

for the *orbit-averaged* subhalo mass loss rate. This avoids having to integrate individual subhalo orbits, as done in other semi-analytical models for dark matter substructure (e.g., Taylor & Babul 2004, 2005a,b; Benson et al. 2002; Taffoni et al. 2003; Oguri & Lee 2004; Zentner & Bullock 2003; Peñarrubia & Benson 2005; Zentner et al. 2005; Gan et al. 2010). We have made a number of improvements and extensions with respect to the original B05 model; in particular, we

- (i) use Monte Carlo merger trees constructed using the method of P08, which, as demonstrated in JB14, yields results in much better agreement with numerical simulations than the Somerville & Kolatt (1999) method used by B05.
- (ii) construct and use complete merger trees, rather than just the mass assembly histories of the main progenitor. This allows us to investigate the statistics of subhaloes of different orders.
- (iii) adopt a new mass loss model, that is calibrated against numerical simulations and which also accounts for the scatter in subhalo mass loss rates that arises from scatter in orbital properties (energy and angular momentum) and (sub)halo concentrations.
- (iv) include a method for converting halo mass to maximum circular velocity, thus allowing us to study subhalo velocity functions as well as subhalo mass functions.

In this paper, the first in a series that addresses the statistics of dark matter subhaloes, we have mainly focussed on the *average* subhalo mass and velocity functions, where the average is taken over large numbers of Monte Carlo realizations for a certain host halo mass, M_0 , redshift, z_0 , and cosmology. Our model has only one free parameters, which sets the overall normalization of the orbit-averaged mass loss rates of dark matter subhaloes. After tuning this pa-

rameter such that the model reproduces the normalization of the evolved SHMF in the numerical simulations of G08, the same model can accurately reproduce the evolved subhalo mass and velocity functions in numerical simulations for host haloes of different mass, in different Λ CDM cosmologies, and for subhaloes of different orders, without having to adjust this parameter.

The inferred orbit-averaged mass loss rates are consistent with the simulation results of G08, and imply that an average dark matter subhalo loses in excess of 80 percent of its infall mass during its first radial orbit within the host halo. More massive subhaloes, in units of the normalized mass, m/M , lose their mass more rapidly due to (i) the concentration-mass relation of dark matter haloes, which causes subhaloes with smaller m/M to be more resilient to tidal stripping, and (ii) dynamical friction, which causes more massive subhaloes to lose more orbital energy and angular momentum, resulting in enhanced stripping. According to our mass loss model, subhaloes with an infall mass that is 10 percent of the host halo mass will lose on average more than 95 percent of their infall mass during their first radial orbital period.

One of the main findings of this paper is that the average subhalo mass and velocity functions, both evolved and unevolved, can be accurately fit by a simple Schechter-like function of the form

$$\frac{dN}{d \ln \psi} = \gamma (\psi)^\alpha \exp[-\beta(\psi)^\omega]. \quad (36)$$

where, depending on which function is being considered, ψ is m/M_0 , m_a/M_0 , $V_{\text{max}}/V_{\text{vir},0}$, or $V_{\text{acc}}/V_{\text{vir},0}$. In particular, restricting ourselves to Λ CDM cosmologies with parameters that are consistent with recent constraints within a factor of roughly two, we find that

- The *unevolved* SHMF is (close to) universal, with the parameters ($\alpha, \beta, \gamma, \omega$) independent of host halo mass, redshift and cosmology (see also B05; Li & Mo 2009; Yang et al. 2011). We emphasize, though, that although the functional form of Eq. (36) can adequately describe this universal unevolved SHMF, it is more accurately described by the double-Schechter-like function presented in JB14.

- The *evolved* SHMF has a universal shape (i.e., fixed α, β and ω), which is accurately described by Eq. (36), but with a normalization, γ , that depends on host halo mass, redshift and cosmology. We have demonstrated that γ is tightly correlated with the ‘dynamical age’ of the host halo, defined as the number of halo dynamical times that have elapsed since its formation (i.e., since redshift $z_{1/2}$ at which the host halo’s main progenitor reaches a mass equal to $M_0/2$). Using this relation we have presented a universal fitting function for the average, evolved SHMF that is valid for any host halo mass, at any redshift, and for any Λ CDM cosmology. The corresponding power-law slopes, α , are -0.78 , -0.93 and -0.82 for first-order subhaloes, second-order subhaloes (i.e., sub-subhaloes), and for subhaloes of all orders, significantly shallower than what has been claimed in numerous studies based on numerical simulations (see Paper II for a detailed discussion).

- Unlike the unevolved mass function, the *unevolved* SHVF is not universal, in that the parameter β is found to depend on host mass, redshift and cosmology. This has its origin in the concentration-mass-redshift relation of dark matter haloes, and can be accounted for by replacing ψ in Eq. (36) with $a\psi$, where a is a (universal) scale factor given by $a \propto V_{\text{vir}}(M_0/40, z_0)/V_{\text{max}}(M_0/40, z_{0.25})$. When using this simple rescaling, one obtains a universal fitting function for the unevolved SHVF whose parameters α, β, γ and ω are independent of host mass, redshift and cosmology. Note that this unevolved SHVF is one of the key ingredients in the popular method of subhalo abundance matching.

- Taking into account both the ‘dynamical age’-dependence of the normalization of the evolved SHMF and the ‘ a ’-scaling of the unevolved SHVF, also yields a universal fitting function for the *evolved* SHVF. In this case we find that the power-law slope for the evolved SHVF of all orders is equal to $\alpha = -2.6$.

The various, universal fitting functions for the subhalo mass and velocity functions presented here, and summarized in Appendix A, can be used to quickly compute the average abundance of subhaloes of given mass or maximum circular velocity, at any redshift, and for any (reasonable) Λ CDM cosmology, without having to run and analyze high resolution numerical simulations. In the second paper in this series (van den Bosch & Jiang 2014), we compare subhalo mass and velocity functions obtained from different simulations and with different subhalo finders, among each other, and with predictions from our semi-analytical model. We demonstrate that our model is in excellent agreement with simulation results that analyze their data with halo finders that use the full 6D phase-space information (e.g., **ROCKSTAR**), or that use temporal information (e.g., **SURV**). Results obtained using subhalo finders that only rely on the densities in configuration space are shown to dramatically underpredict the abundance of massive subhaloes, by more than an order of magnitude. In the third paper in this series (Jiang & van

den Bosch, in preparation), we use our model to investigate, in unprecedented detail, the halo-to-halo variance of dark matter substructure, which is important, among others, for assessing the severity of the ‘too-big-to-fail’ problem (see also Purcell & Zentner 2012).

ACKNOWLEDGMENTS

We are grateful to Andrew Wetzel and Mike Boylan-Kolchin for helpful discussions and to Hao-Yu Wu for sharing some of their data from the Rhapsody simulation project. We also thank the people behind the MultiDark simulation for making their halo catalogs publicly available, and the organizers of the program “First Galaxies and Faint Dwarfs: Clues to the Small Scale Structure of Cold Dark Matter” held at the Kavli Institute for Theoretical Physics (KITP) in Santa Barbara, for creating a stimulating, interactive environment that started the research presented in this paper, and the KITP staff for all their help and hospitality. This research was supported in part by the National Science Foundation under Grant No. PHY11-25915.

REFERENCES

- Behroozi P. S., Wechsler R. H., Wu H.-Y., 2013a, *ApJ*, 762, 109
 Behroozi P. S., Wechsler R. H., Wu H.-Y., Busha M.T., Klypin A.A., Primack J.R., 2013b, *ApJ*, 763, 18
 Benson A. J., Frenk C. S., Lacey C. G., Baugh C. M., Cole S., 2002, *MNRAS*, 333, 177
 Binney J., Tremaine S., 2008, *Galactic Dynamics*, Princeton University Press
 Bradač M., Schneider P., Steinmetz M., Lombardi M., King L. J., Porcas R., 2002, *A&A*, 388, 373
 Bond J. R., Cole S., Efstathiou G., Kaiser N., 1991, *ApJ*, 379, 440
 Boylan-Kolchin M., Bullock J. S., Kaplinghat M., 2011, *MNRAS*, 415, L40
 Bryan G. L., Norman M. L., 1998, *ApJ*, 495, 80
 Carlberg R. G., 2009, *ApJ*, 705L, 223
 Cole S., Lacey C. G., Baugh C. M., Frenk C. S., 2000, *MNRAS*, 319, 168
 Cole S., Helly J., Frenk C. S., Parkinson H., 2008, *MNRAS*, 383, 546
 Conroy C., Wechsler R. H., Kravtsov A. V., 2006, *ApJ*, 647, 201
 Conroy C., Wechsler R. H., Kravtsov A. V., 2007, *ApJ*, 668, 826
 Dalal N., Kochanek C. S., 2002, *ApJ*, 572, 25
 De Lucia G., Kauffmann G., Springel V., White S. D. M., Lanzoni B., Stoeckl F., Tormen G., Yoshida N., 2004, *MNRAS*, 348, 333
 Diemand J., Moore B., Stadel J., 2004, *MNRAS*, 352, 535
 Diemand J., Kuhlen M., Madau P., 2007, *ApJ*, 657, 262
 Fakhouri, O., Ma, C.-P., 2008, *MNRAS*, 386, 577
 Gan J., Kang X., van den Bosch F. C., Hou J., 2010, *MNRAS*, 408, 2201
 Gao L., White S. D. M., Jenkins A., Stoeckl F., Springel V., 2004, *MNRAS*, 355, 819
 Genel S., Genzel R., Bouché N., Naab T., Sternberg A., 2009, *ApJ*, 701, 2002
 Ghigna S., Moore B., Governato F., Lake G., Quinn T., Stadel J., 1998, *MNRAS*, 300, 146
 Ghigna S., Moore B., Governato F., Lake G., Quinn T., Stadel J., 2000, *ApJ*, 544, 616
 Giocoli C., Tormen G., van den Bosch F. C., 2008a, *MNRAS*, 386, 2135 [G08]
 Giocoli C., Pieri L., Tormen G., 2008b, *MNRAS*, 387, 689

- Giocoli C., Tormen G., Sheth R. K., van den Bosch F. C., 2010, MNRAS, 404, 502
- Giocoli C., Tormen G., Sheth R. K., 2012, MNRAS, 422, 185 [G12]
- Gill S. P. D., Knebe A., Gibson B. K., 2004a, MNRAS, 351, 399
- Gill S. P. D., Knebe A., Gibson B. K., Dopita M. A., 2004b, MNRAS, 351, 410
- Guo Q., White S., Boylan-Kolchin M., De Lucia G., Kauffmann G., Lemson G., Li C., Springel V., Weinmann S., 2011, MNRAS, 413, 101
- Hayashi E., Navarro J. F., Taylor J. E., Stadel J., Quinn T., 2003, ApJ, 584, 541
- Hearin A. P., Zentner A. R., Berlind A. A., Newman J. A., 2013, MNRAS, 433, 659
- Ibata R. A., Lewis G. F., Irwin M. J., Quinn T., 2002, MNRAS, 332, 915
- Jiang F., van den Bosch F. C., 2014, MNRAS, in press (arXiv:1311.5225) [JB14]
- Keeton C. R., Moustakas L. A., 2009, ApJ, 699, 1720
- Khochfar S., Burkert A., 2006, A&A, 445, 403
- King I., 1962, AJ, 67, 471
- Knebe A., Knollmann S. R., Muldrew S. I., Pearce F. R., Aragon-Calvo M. A., Ascasibar Y., Behroozi P. S., Ceverino D., 2011, MNRAS, 415, 2293
- Knebe A., Pearce F. R., Lux H., Ascasibar Y., Behroozi P. S., Casado J., Moran C. C., Diemand J., 2013, MNRAS, 435, 1618
- Klypin A., Gottlöber S., Kravtsov A. V., Khokhlov A. M., 1999, ApJ, 516, 530
- Klypin A., Kravtsov A. V., Valenzuela O., Prada F., 1999, ApJ, 522, 82
- Klypin A. A., Trujillo-Gomez S., Primack J. R., 2011, ApJ, 740, 102
- Kravtsov A. V., Berlind A. A., Wechsler R. H., Klypin A. A., Gottlöber S., Allgood B., Primack J. R., 2004, ApJ, 609, 35
- Li Y., Mo H. J., 2009, preprint (arXiv:0908.0301)
- Ludlow A. D., Navarro J. F., Boylan-Kolchin M., Bett P. E., Angulo R. E., Li M., White S. D. M., Frenk C. et al., 2013, MNRAS, 432, 1103
- Macciò A. V., Kang X., Fontanot F., Somerville R. S., Koposov S., Monaco P., 2010, MNRAS, 402, 1995
- Metcalf R. B., Madau P., 2001, ApJ, 563, 9
- Mo H., van den Bosch F. C., White S. D. M., 2010, Galaxy Formation and Evolution, Cambridge University Press
- Moore B., Governato F., Quinn T., Stadel J., Lake G., 1998, ApJ, 499, L5
- Moore B., Ghigna S., Governato F., Lake G., Quinn T., Stadel J., Tozzi P., 1999, ApJ, 524, L19
- Navarro J. F., Frenk C. S., White S. D. M., 1997, ApJ, 490, 493
- Neto A. F., Gao L., Bett P., Cole S., Navarro J. F., Frenk C. S., White S. D. M., Springel V., et al., 2007, MNRAS, 381, 1450
- Oguri, M., Lee, J., 2004, MNRAS, 355, 120
- Parkinson, H., Cole, S., Helly, J., 2008, MNRAS, 383, 557 [P08]
- Peñarrubia J., Benson A. J., 2005, MNRAS, 364, 977
- Peñarrubia J., Navarro J. F., McConnachie A. W., 2008, ApJ, 673, 226
- Peñarrubia J., Benson A. J., Walker M. G., Gilmore G., McConnachie A. W., Mayer L., 2010, MNRAS, 406, 1290
- Pieri L., Bertone G., Branchini E., 2008, MNRAS, 384, 1627
- Prada F., Klypin A. A., Cuesta A. J., Betancort-Rijo J. E., Primack J., 2012, MNRAS, 423, 3018
- Purcell C. W., Zentner A. R., 2012, JCAP, 12, 007
- Onions J., Knebe A., Pearce F. R., Muldrew S. I., Lux H., Knollmann S. R., Ascasibar Y., Behroozi P. et al., 2012, MNRAS, 423, 1200
- Reed D., Governato F., Quinn T., Gardner J., Stadel J., Lake G., 2005, MNRAS, 359, 1537
- Riebe K., et al., 2013, Astron. Nachrichten, 334, 691
- Somerville R. S., Kolatt T. S., 1999, MNRAS, 305, 1
- Stoehr F., White S. D. M., Tormen G., Springel V., 2002, MNRAS, 335, L84
- Taffoni G., Mayer L., Colpi M., Governato F., 2003, MNRAS, 341, 434
- Taylor J. E., Babul A., 2001, ApJ, 559, 716
- Taylor J. E., Babul A., 2004, MNRAS, 348, 811
- Taylor J. E., Babul A., 2005a, MNRAS, 364, 515
- Taylor J. E., Babul A., 2005b, MNRAS, 364, 535
- Tormen G., 1997, MNRAS, 290, 411
- Tormen G., Diaferio A., Syer D., 1998, MNRAS, 299, 728
- Tormen G., Moscardini L., Yoshida N., 2004, MNRAS, 350, 1397
- Tóth G., Ostriker J. P., 1992, ApJ, 389, 5
- Vale A., Ostriker J. P., 2004, MNRAS, 353, 189
- van den Bosch, F. C., Tormen, G., Giocoli, C., 2005, MNRAS, 359, 1029 [B05]
- van den Bosch, F. C., Jiang F., 2014, MNRAS, submitted
- von Hoerner S., 1957, ApJ, 125, 451
- Wang H. Y., Jing Y. P., Mao S., Kang X., 2005, MNRAS, 364, 424
- Weinberg D. H., Colombi S., Davé R., Katz N., 2008, ApJ, 678, 6
- Wetzel A. R., 2011, MNRAS, 412, 49
- Wechsler R. H., Bullock J. S., Primack J. R., Kravtsov A. V., Dekel A., 2002, ApJ, 568, 52
- Wu H.-Y., Hahn O., Wechsler R. H., Mao Y.-Y., Behroozi P. S., 2013a, ApJ, 763, 70
- Wu H.-Y., Hahn O., Wechsler R. H., Behroozi P. S., Mao Y.-Y., 2013b, ApJ, 767, 23
- Yang X., Mo H. J., Zhang Y., van den Bosch F. C., 2011, ApJ, 741, 13
- Zentner A. R., Bullock J. S., 2003, ApJ, 598, 49
- Zentner A. R., Berlind A. A., Bullock J. S., Kravtsov A. V., Wechsler R. H., 2005, ApJ, 624, 505
- Zhao D. H., Jing Y. P., Mo H. J., Börner G., 2009, ApJ, 707, 354

APPENDIX A: UNIVERSAL FITTING FUNCTIONS FOR THE SUBHALO MASS AND VELOCITY FUNCTIONS

This appendix describes how to compute an average mass or velocity function (evolved or unevolved) for subhaloes of all orders. We have shown in §4 that the average evolved and unevolved subhalo mass and velocity functions of a host halo of mass M_0 at redshift z_0 are well described by the general fitting function

$$\frac{dN}{d \ln \psi} = \gamma (a\psi)^\alpha \exp[-\beta (a\psi)^\omega], \quad (\text{A1})$$

where ψ stands for the corresponding quantity; m_{acc}/M_0 , m/M_0 , $V_{\text{acc}}/V_{\text{vir},0}$, or $V_{\text{max}}/V_{\text{vir},0}$. For subhaloes of all orders, the corresponding best-fit values for α , β , γ , ω and a are listed in Table A1. As is evident, they are completely described by the subhalo mass fraction f_s and the scale parameter a . In what follows we outline the steps required to compute these two values for a host halo of mass M_0 at redshift z_0 in a given Λ CDM cosmology:

(i) Obtain the redshift z_f , by which the main progenitor has assembled a fraction f of its final mass M_0 at redshift z_0 . In particular, compute z_f for $f = 0.5$, 0.25 , and 0.04 using the G12 model for formation redshift, by solving for the root of

$$\delta_c(z_f) = \delta_c(z_0) + \tilde{w}_f \sqrt{\sigma^2(fM_0) - \sigma^2(M_0)}, \quad (\text{A2})$$

Table A1. Parameters for universal SHMF and SHVF.

| ψ (1) | γ (2) | α (3) | β (4) | ω (5) | a (6) |
|-----------------------------------|-----------------|-----------------|----------------|-----------------|------------|
| m_{acc}/M_0 | 0.22 | -0.91 | 6 | 3 | 1 |
| m/M_0 | $0.31f_s$ | -0.82 | 50 | 4 | 1 |
| $V_{\text{acc}}/V_{\text{vir},0}$ | 2.05 | -3.2 | 2.2 | 13 | Eq.(A3) |
| $V_{\text{max}}/V_{\text{vir},0}$ | $5.45f_s^{1.4}$ | -2.6 | 4 | 15 | Eq.(A3) |

where $\tilde{w}_f = \sqrt{2 \ln(\alpha_f + 1)}$ and $\alpha_f = 0.815e^{-2f^3}/f^{0.707}$.

(ii) Compute the ‘dynamical age’, N_τ , of the host halo using Eq. (24) with $z_{\text{form}} = z_{0.5}$. Use this to infer the subhalo mass fraction, f_s , from Eq.(26).

(iii) Compute the scale parameter, a , given by

$$a = 1.536 \frac{V_{\text{vir}}(M_0/40, z_0)}{V_{\text{max}}(M_0/40, z_{0.25})}, \quad (\text{A3})$$

with V_{vir} and V_{max} given by Eqs. (17) and (16), respectively, and with $z_{0.25}$ obtained in step (i). Note that the computation of V_{max} requires the halo concentration parameter, c , which can be computed from the $z_{0.04}$ obtained under step (i) using the concentration-mass-redshift relation of Zhao et al. (2009), given by Eq. (18).

Although we believe this ‘recipe’ to be reliable for host haloes that cover a wide range in halo masses and redshifts, and for a wide range of cosmologies, we caution that we have only been able to test it against numerical simulations over the mass range $10^{11} h^{-1} \text{M}_\odot \lesssim M_0 \lesssim 10^{15} h^{-1} \text{M}_\odot$ at relatively low redshifts, and for a range of cosmologies that are all similar to the best-fit cosmologies advocated by the recent CMB experiments (see Paper II for details). We therefore caution against using this method blindly for cosmologies and/or halo masses that are very different from those mentioned above. Finally, we mention that the fitting function for the *unevolved* SHMF described by the parameters in Table A1 is less accurate than that presented in JB14. Hence, if accuracy is a concern, we recommend the latter over the one presented here.